JAEA-Research
2006-071

JAEA-Research

Evaluation of Deuteron-induced Activation for IFMIF Accelerator Structural Materials

Makoto NAKAO, Jun-ichi HORI*
Kentaro OCHIAI, Naoyoshi KUBOTA
Satoshi SATO, Michinori YAMAUCHI
Noriko S. ISHIOKA, Hiroyuki SUDO
and Takeo NISHITANI

Fusion Neutronics Group
Fusion Research and Development Directorate

November 2006

Japan Atomic Energy Agency

日本原子力研究開発機構

本レポートは日本原子力研究開発機構が不定期に発行する成果報告書です。
本レポートの入手並びに著作権利用に関するお問い合わせは、下記あてにお問い合わせ下さい。
なお、本レポートの全文は日本原子力研究開発機構ホームページ（http://www.jaea.go.jp/index.shtml）より発信されています。このほか財団法人原子力弘済会資料センター*では実費による複写頒布を行っております。

〒319-1195　茨城県那珂郡東海村白方白根 2 番地 4
日本原子力研究開発機構　研究技術情報部　研究技術情報課
電話 029-282—6387, Fax 029-282-5920

*〒319-1195　茨城県那珂郡東海村白方白根 2 番地 4　日本原子力研究開発機構内

This report is issued irregularly by Japan Atomic Energy Agency
Inquiries about availability and/or copyright of this report should be addressed to
Intellectual Resources Section, Intellectual Resources Department,
Japan Atomic Energy Agency
2-4 Shirakata Shirane, Tokai-mura, Naka-gun, Ibaraki-ken 319-1195 Japan
Tel +81-29-282-6387, Fax　+81-29-282-5901

JAEA-Research 2006-071

Evaluation of Deuteron-induced Activation for IFMIF Accelerator Structural Materials

Makoto NAKAO, Jun-ichi HORI*, Kentaro OCHIAI, Naoyoshi KUBOTA※, Satoshi SATO
Michinori YAMAUCHI, Noriko S. ISHIOKA+, Hiroyuki SUDO+ and Takeo NISHITANI

Division of Fusion Energy Technology
Fusion Research and Development Directorate
Japan Atomic Energy Agency
Naka-shi, Ibaraki-ken

(Received October 2, 2006)

The International Fusion Materials Irradiation Facility (IFMIF) is a neutron source facility designed to produce an intense neutron field for irradiation test of fusion reactor candidate materials. In the design of IFMIF, long-term operation with total facility availability of at least 70 % is required. However, activation of structural materials by deuteron beam limits maintenance, which causes lower facility availability. Thus it is essential to prepare deuteron-induced activation cross section database and to select low activation materials based on it. In this work, we measured deuteron-induced activation cross sections of aluminum, vanadium, chromium, manganese, iron, nickel, copper, tantalum, tungsten and gold. The measured cross sections were compared with other experimental data and calculations. Deuteron-induced activities of nuclides produced in SS316 and F82H alloys used as the accelerator structural material were also measured to validate the measured cross sections comprehensively. It demonstrated that the measured activities of almost all the nuclides were in agreement with evaluated ones based on the measured cross sections within error.

Keywords: IFMIF, Deuteron, Activation Cross Section, TIARA, Induced Activity

＋Radiation-Applied Biology Division, Quantum Beam Science Directorate
※Post-Doctoral Fellow
＊Kyoto University

IFMIF 加速器構成材料の重陽子入射による放射化の評価

日本原子力研究開発機構　核融合研究開発部門
核融合エネルギー工学研究開発ユニット
中尾　誠, 堀　順一*, 落合　謙太郎, 久保田　直義※, 佐藤　聡
山内　通則, 石岡　典子+, 須藤　広行+, 西谷　健夫

(2006 年 10 月 2 日受理)

国際核融合材料照射施設（IFMIF）は核融合候補材料照射試験を行うための強力中性子源として計画中の施設である. この施設では加速器稼働率 70 %を目指しているが, 重陽子による加速器構成材料の放射化によってメンテナンス作業が制限されることが, 稼働率を低下させる要因となる. したがって, 重陽子入射に対する精度の良い放射化断面積データベースを整備し, それを基に低放射化材料を選択することが不可欠である. 本研究では, 加速器構成材料であるアルミニウム, バナジウム, クロム, マンガン, 鉄, ニッケル, 銅, タンタル, タングステン及び金の放射化断面積を測定し, 他の実測値, 計算値と比較した. また, 測定した放射化断面積の妥当性を総合的に判断するため, 実際に加速器で使用される SUS316, F82H への重陽子入射によって生成する核種の放射能の測定も行った. 測定対象としたほぼ全ての核種の放射能は, 測定した断面積を基に評価した放射能と誤差の範囲で一致することを示した.

那珂核融合研究所（駐在）: 〒319-0193　茨城県那珂市向山 801-1
＋量子ビーム応用研究部門バイオ応用技術研究ユニット
※博士研究員
＊京都大学

Contents

目 次

List of Tables and Figures

1. Introduction

The International Fusion Materials Irradiation Facility (IFMIF)[1] is an accelerator-based D-Li neutron source designed to produce an intense neutron field for testing fusion reactor candidate materials. The IFMIF has two 40 MeV deuteron linear accelerators with each 125 mA beam current. Figure 1 shows a bird view of the IFMIF.

In the design of IFMIF, long-term operation with total facility availability of at least 70 % is required. However, activation of structural materials along the beam transport lines by deuteron beam loss prolongs the cooling time for maintenance, which causes lower facility availability. Thus it is essential to prepare deuteron-induced activation cross section database in order to select structural materials and determine the beam loss criteria to reduce activations based on it. In particular, cross sections of radioactive products with half-lives greater than several minutes are important because their nuclides determine cooling time for maintenance.

In this work, we performed deuteron irradiation experiments to measure two kinds of data for IFMIF accelerator structural materials. One is a measurement of deuteron-induced activation cross sections for pure metal materials, *i.e.* aluminum, vanadium, chromium, manganese, iron, nickel, copper, tantalum, tungsten and gold, in the energy range of 14-49 MeV. Aluminum is the main material of the beam tube and chamber. Vanadium is the corrosion material in Li target. Chromium and manganese are contained in SS316 and F82H. Iron is the inner material of drift tube and major component of SS316 and F82H. Nickel is the corrosion material in Li target and contained in SS316. Copper is used in the cavity walls, electrodes and magnetic conductors. Tantalum, tungsten and gold were chosen because high-Z materials are candidate for beam slits and coatings to protect the beam facing materials.

The other is a measurement of deuteron-induced activities of nuclide produced in SS316 and F82H by 39.5 MeV deuteron. The both alloys are used mainly as structural materials and especially also used as an assembly around liquid lithium target. We intend to be the experimental verification of estimated activities with the measured activation cross sections for pure materials in the alloys.

2. Experimental procedure

2.1 Deuteron irradiation

The deuteron irradiation experiment was performed at the LA1 station of an AVF cyclotron in the Takasaki Ion accelerators for Advanced Radiation Application (TIARA) facility. Figures 2 and 3 show a bird view of TIARA and beam transport lines of the cyclotron, respectively. In this experiment, we adopted a stacked-foil activation technique to measure cross sections at different energy points simultaneously. The stacked-foil consisted of some kinds of materials which produce radioactive nuclides with different half-lives, which made the following activity measurement effective. For example, a stacked-foil with a twenty-layer structure was Ta, Ni, Fe, V, Ta, Ni, Fe, V, Ta, Ni, Fe, V, Ta, Ni, Fe, V, Ta, Ni, Fe and Cu. Each foil with thicknesses of 10-200 μm was cut into a 10 mm squared sample. The purities of pure metal foils were more than 99 %, which is listed in Table 1. The samples wrapped in an aluminum cover of 10 μm in thickness were set in the stack folder, which is held with an aluminum stopper of 100 μm in thickness as shown in Fig. 4. The LA1 port was evacuated by a turbo-molecular

pump to a base pressure of 1×10^{-5} Pa. The stack holder was cooled by water. The stacked-foil was irradiated with the deuteron beam on normal incidence with the current of 0.1 μA(beam spot size: 8 mm in diameter) during 2-7 minutes. Incident energies of 25, 35, 41 and 50 MeV were chosen. After the irradiation and suitable cooling time, gamma-rays emitted from the irradiated samples were measured by a High-Purity Germanium (HPGe) detector.

In the same way, activities of nuclides produced in SS316 and F82H were measured by 39.5 MeV deuteron (incident deuteron energy: 41 MeV). The composition of SS316 and F82H alloys is listed in Table 2. The thickness of the samples is 100 μm.

2.2 Data processing

The activation cross section, σ(E), at the incident deuteron energy, E, in laboratory system was calculated with the following equation;

$$\sigma(E)=\frac{\lambda Y_{\mathrm{photo}}}{N\int\phi(E)dE\left(1-e^{-\lambda t_i}\right)e^{-\lambda t_c}\left(1-e^{-\lambda t_m}\right)\varepsilon_f I_\gamma},$$

where

Y_{photo} : gamma-ray yield of the photo peak,
N : number of target atoms in the irradiation sample,
$\phi(E)$: incident deuteron fluence rate,
λ : decay constant,
t_{i} : deuteron irradiation time,
t_{m} : gamma-ray measurement time,
t_{c} : cooling time,
ε_{f} : detection efficiency of the HPGe detector,
I_γ : emission intensity of gamma-ray pre decay.

The energy E was the averaged value derived from the energy loss in the sample, which was calculated by OSCAR code based on the Ziegler's empirical formula in the IRACM code system[2]. The fluence rate $\phi(E)$ was computed from measured ^{65}Zn activities and the $^{\mathrm{nat}}$Cu(d,x)^{65}Zn reaction cross section data reported by Takacs et al. [3]

A typical gamma-ray spectrum emitted from a Cu sample is shown in Fig. 5. There are four photo-peaks at 596, 655, 669 and 1345 keV arising from ^{62}Zn, ^{61}Cu, ^{63}Zn and ^{64}Cu activities, respectively. The activation cross sections were derived from these photo-peak yields of gamma-rays.

Error sources of the measured activation cross sections are due to statistical accuracy of a photo peak yield, continuous background countings of other gamma-rays such as Compton continuum, the cross section of the $^{\mathrm{nat}}$Cu(d,x)^{65}Zn reaction, the full energy detection efficiency of the HPGe detector and the estimated number of the target atom in the beam spot area. The total error of the measured activation cross sections was 10-20 % except for the case of a small Y_{photo} under large countings of background gamma-rays.

3. Results and discussion

Activation cross section data measured in this work were compared with previous experimental data measured by other groups and two types of calculation ones. Data in the EXFOR database were cited as the previous experimental data. Calculation values were the data library (ACSELAM) computed by the ALICE-F code[4] and are computed by the TALYS code[5] (TALYS). Since both the calculated values are given for each isotope, data normalized by weighting with natural abundance are used for the comparison.

3.1 Activation cross sections for pure metal materials

3.1.1 Aluminum

The cross sections of $^{27}Al(d,x)^{22}Na$, $^{27}Al(d,x)^{24}Na$ and $^{27}Al(d,2p)^{27}Mg$ reactions in aluminum have been measured. The half-lives of ^{22}Na, ^{24}Na and ^{27}Mg are 2.6 years, 15.0 hours and 9.5 minutes, respectively. The result for the $^{27}Al(d,x)^{22}Na$ reaction is shown in Fig. 6. The present data correspond with the previous ones by Martens et al.[6], Michel et al.[7] and Takacs et al.[3] within 40 %. ACSELAM is smaller than the present data by a factor of 2-8. TALYS agrees with the present data within 60 %. The cross sections of the $^{27}Al(d,x)^{24}Na$ reaction are shown in Fig. 7. The present data also correspond with the data previous ones by the same authors within 40 %. ACSELAM is smaller than the present data by a factor of 2-13. TALYS is in good agreement with the present data above 35 MeV and is larger than the present data by a factor of 2-3 below 30 MeV. The cross section of the $^{27}Al(d,2p)^{27}Mg$ reaction is shown in Fig. 8. The previous cross section was only measured by Wilson et al.[8] below 16 MeV. ACSELAM corresponds with the present data within a factor of 2. TALYS agrees with the present data within 30 % above 35 MeV and is larger than the present data by a factor of 1-4 below 30 MeV.

3.1.2 Vanadium

The $^{51}V(d,4n)^{49}Cr$ (42.3 minutes half-life) reaction cross section has been measured, as is shown in Fig. 9. Weinreich et al.[9] only reported the data of this reaction above 32 MeV, which is smaller than the present data by a factor of 2. ACSELAM is larger than the present data by a factor of 4-6. TALYS is smaller than the present data by 2 orders of magnitude.

3.1.3 Chromium

Natural chromium includes four stable isotopes, *i.e.* ^{50}Cr(4.34 %), ^{52}Cr(83.79 %), ^{53}Cr(9.50 %) and ^{54}Cr(2.37 %). The cross sections of the $^{nat}Cr(d,x)^{48}V$ and $^{nat}Cr(d,x)^{52}Mn$ reactions at 39.5 MeV are listed in Table 3. The half-lives of ^{48}V and ^{52}Mn are 16.0 days and 5.6 days, respectively. No experimental data for both reactions are measured in this energy region. For the $^{nat}Cr(d,x)^{48}V$ reaction, ACSELAM and TALYS correspond with the present data within 60 % and 50 %, respectively. For the $^{nat}Cr(d,x)^{52}Mn$ reaction, ACSELAM is larger than the present data by a factor of 2 and TALYS agrees with the present data within 40 %.

3.1.4 Manganese

The cross section of the $^{55}Mn(d,x)^{54}Mn$ (312.1 days half-life) reaction at 39.5 MeV is also listed in Table 3. There is no previous experimental data. ACSELAM and TALYS are roughly in agreement with the present data by 60 % and 30 %, respectively.

3.1.5 Iron

Natural iron is composed of ^{54}Fe(5.81 %), ^{56}Fe(91.72 %), ^{57}Fe(2.21 %) and ^{58}Fe(0.28 %). The measured cross sections of the ^{nat}Fe(d,x)^{52}Mn, ^{nat}Fe(d,x)^{54}Mn, ^{nat}Fe(d,x)^{55}Co, ^{nat}Fe(d,x)^{56}Co and ^{nat}Fe(d,x)^{57}Co reactions are shown in Figs. 10, 11, 12, 13 and 14, respectively. The half-lives of produced nuclides ^{55}Co, ^{56}Co and ^{57}Co are 17.5 hours, 77.2 days and 271.8 days. The previous experimental data were reported by Clark et al.[10] and Hermanne et al.[11] for ^{nat}Fe(d,x)^{52}Mn, ^{nat}Fe(d,x)^{54}Mn, ^{nat}Fe(d,x)^{55}Co and ^{nat}Fe(d,x)^{57}Co. Note that ^{nat}Fe(d,x)^{54}Mn, ^{nat}Fe(d,x)^{55}Co and ^{nat}Fe(d,x)^{57}Co data in Ref. 10 were smoothed ones fitted to the experimental results. Clark et al.[10] and Takacs et al.[3] reported the data of ^{nat}Fe(d,x)^{56}Co. For the ^{nat}Fe(d,x)^{52}Mn reaction, the present data correspond with both the previous experimental and calculated data within 50 %. For the ^{nat}Fe(d,x)^{54}Mn reaction, the present data agree with the previous experimental data within 50 %. ACSELAM is smaller than the present data by a factor of 5. TALYS is in good agreement with the present data above 35 MeV and is smaller than the present data by a factor of 3 below 30 MeV. For the ^{nat}Fe(d,x)^{55}Co reaction, the present data correspond with Clark's data within 30-80% and Hermanne's data within 40 %. ACSELAM is larger than the present data by a factor of 3-8. TALYS corresponds with the present data within 40 %. For the ^{nat}Fe(d,x)^{56}Co reaction, the present data agree with the Clark's one above 27 MeV and the Takacs's one. ACSELAM is larger than the present data by a factor of 2 and TALYS corresponds with the present data within 50 %. For the ^{nat}Fe(d,x)^{57}Co reaction, the present data agree with the previous ones within 60 %. ACSELAM is larger than the present data by a factor of 1-3 and TALYS is smaller than the present data by a factor of 2-3.

3.1.6 Nickel

We obtain the cross sections of the ^{nat}Ni(d,x)^{55}Co, ^{nat}Ni(d,x)^{56}Co, ^{nat}Ni(d,x)^{57}Co, ^{nat}Ni(d,x)^{60}Cu and ^{nat}Ni(d,x)^{61}Cu reactions in natural nickel(^{58}Ni: 68.08 %, ^{60}Ni: 26.22 %, ^{61}Ni: 1.14 %, ^{62}Ni: 3.63 %). The half-lives of ^{60}Cu and ^{61}Cu are 23.7 minutes and 3.3 hours. The cross section of the ^{nat}Ni(d,x)^{55}Co reaction is shown in Fig. 15. The present data agree with the previous one reported by Cline et al.[12] The difference among the present and both calculated data with the same tendency is less than a factor of 2. The cross section value for the ^{nat}Ni (d,x)^{56}Co reaction at 39.5 MeV is indicated in Table 3. ACSELAM is in good agreement with the present data and TALYS corresponds with the present data within 70 %. Figure 16 shows the cross section of the ^{nat}Ni(d,x)^{57}Co reaction. The previous data and TALYS correspond with the present data within 40 % and 80 %, respectively. ACSELAM is smaller than the present data by a factor of 2-4. Figure 17 shows the cross section of the ^{nat}Ni(d,x)^{60}Cu reaction. There is no previous experimental data for the reaction. ACSELAM is larger than the present data by a factor of 1-7. TALYS corresponds with the present data within 70 %. For the ^{nat}Ni(d,x)^{61}Cu reaction, the present data are in good agreement with the data by Takacs et al.[3], which is shown in Fig. 18. ACSELAM is larger than the present data by a factor of 1-3. TALYS is smaller than the present data by a factor of 2-3.

3.1.7 Copper

Natural copper is composed of ^{63}Cu(69.17 %) and ^{65}Cu(30.83 %). The measured cross sections of the ^{nat}Cu(d,x)^{62}Zn, ^{nat}Cu(d,x)^{63}Zn, ^{nat}Cu(d,x)^{61}Cu and ^{nat}Cu(d,x)^{64}Cu reactions are shown in Figs. 19, 20, 21 and 22, respectively. The half-lives of ^{62}Zn, ^{63}Zn, ^{61}Cu and ^{64}Cu are 9.2 hours, 38.5 minutes, 3.3 hours and 12.7 hours. The previous data were reported by Bartell et al.[13] and Fulmer et al.[14] For ^{nat}Cu(d,x)^{62}Zn, Fulmer's data are larger than the present one by a factor of 2-3. ACSELAM is also larger than the present data by a factor of 2-3. TALYS below 25 MeV is in good agreement with the present data although that

above 30 MeV is smaller than the present one by a factor of 2-3. For $^{nat}Cu(d,x)^{63}Zn$, Fulmer's data are larger than the present one by a factor of 2. ACSELAM corresponds with the present data within 40 %. TALYS is smaller than the present data by a factor of 2-3. For $^{nat}Cu(d,x)^{61}Cu$, Fulmer's data are larger than the present one by a factor of 1-6. ACSELAM and TALYS are larger than the present data by a factor of 2-3 and 1-3, respectively. For $^{nat}Cu(d,x)^{64}Cu$, Fulmer's and both calculated data correspond with the present one within 60 % and 80 %, respectively.

3.1.8 Tantalum

The cross sections of the $^{181}Ta(d,x)^{178}Ta$ (2.4 hours half-life) and $^{181}Ta(d,x)^{180}Ta$ (8.2 hours half-life) reactions are measured. Figure 23 shows the $^{181}Ta(d,x)^{178}Ta$ cross section. There is one measurement by Bisplinghoff et al.[15] above 42 MeV, which are 3 times as small as the present data. ACSELAM and TALYS are larger than the present data by a factor of 2-6. Figure 24 shows the $^{181}Ta(d,x)^{180}Ta$ cross section. There is no previous experimental data for this reaction. ACSELAM and TALYS are half of the present data.

3.1.9 Tungsten

Natural tungsten is composed of ^{180}W(0.12 %), ^{182}W(26.50 %), ^{183}W(14.31 %), ^{184}W(30.64 %) and ^{186}W(28.43 %). The cross sections of eight reactions, *i.e.* $^{nat}W(d,x)^{181}Re$, $^{nat}W(d,x)^{182m}Re$, $^{nat}W(d,x)^{182g}Re$, $^{nat}W(d,x)^{183}Re$, $^{nat}W(d,x)^{184m}Re$, $^{nat}W(d,x)^{184g}Re$, $^{nat}W(d,x)^{186}Re$ and $^{nat}W(d,x)^{187}W$, have been measured in this work. The half-lives of ^{181}Re, ^{182m}Re, ^{182g}Re, ^{183}Re, ^{184m}Re, ^{184g}Re, ^{186}Re and ^{187}W are 19.9 hours, 12.7 hours, 2.7 days, 70.0 days, 169 days, 38.0 days, 3.8 days and 23.7 hours, respectively. As the previous experimental data, the data reported by Tarkanyi et al.[16] are compared to the present data. As for the $^{nat}W(d,x)^{181}Re$ cross section shown in Fig. 25, the present data correspond with the previous one within 40 %. ACSELAM and TALYS also agree with the present data within 70 % and 40 %. Figure 26 shows the cross sections of both $^{nat}W(d,x)^{182m}Re$ and $^{nat}W(d,x)^{182g}Re$ reactions. The present data of both reactions are in good agreement with the previous one. ACSELAM and TALYS correspond with the present data within 50 %. Figure 27 shows the cross section of $^{nat}W(d,x)^{183}Re$. The present data correspond with the previous one within 50 % below 30 MeV and are in good agreement with the previous one above 30 MeV. The both calculated data agree with the present data within 50 %. Figure 28 shows the cross sections of both $^{nat}W(d,x)^{184m}Re$ and $^{nat}W(d,x)^{184g}Re$ reactions. The present data correspond with the previous one within 50 %. TALYS also agrees with the present data within 50 %. ACSELAM is different from the present data in shape above 20 MeV and is smaller than the present data by a factor of 2-7. For $^{nat}W(d,x)^{186}Re$, the present data are in good agreement with the previous data, which is shown in Fig. 29. Both calculated data are larger than the present data by a factor of 1-3 for ACSELAM and 2 for TALYS. For $^{nat}W(d,x)^{187}W$, the present data correspond with the previous one within 60 %, which is shown in Fig. 30. ACSELAM is smaller than the present data by a factor of 1-9 below 40MeV and corresponds with them within 60% above 40MeV. TALYS is smaller than the present data by a factor of 2-4.

3.1.10 Gold

The cross section of the $^{197}Au(d,x)^{194}Au$ (38.0 hours half-life) reaction is shown in Fig. 31. No previous results are found in literatures. ACSELAM and TALYS agree with the present data within 60 %.

3.2 Induced activity of SS316 and F82H

Table 4 shows deuteron induced activity of each nuclide produced in SS316 and F82H by 39.5 MeV deuterons. The evaluated activities are derived from the cross section measured in the present experiment. The averaged deuteron fluxes were 4.09×10^{11} /s for SS316 and 3.86×10^{11} /s for F82H. The irradiation time was both 240 seconds. We considered 6 nuclides produced by 10 reactions, that is ^{48}V (d+^{nat}Cr), ^{52}Mn (d+^{nat}Cr and d+^{nat}Fe), ^{54}Mn (d+^{nat}Fe and d+^{55}Mn), ^{55}Co (d+^{nat}Fe and d+^{nat}Ni), ^{56}Co (d+^{nat}Fe and d+^{nat}Ni), ^{57}Co (d+^{nat}Fe and d+^{nat}Ni) and ^{181}Re (d+^{nat}W). The evaluated activities of ^{48}V, ^{52}Mn, ^{55}Co, ^{56}Co, ^{57}Co in the both alloys, ^{54}Mn in SS316 and ^{181}Re in F82H are in agreement with the measured ones within 14%, whereas that of ^{54}Mn in F82H is overestimated by about 29 %. The difference within 14 % between the measured and evaluated activities in the both alloys is the margin of errors caused by the cross section measurements. We could not identify cause of the discrepancy for ^{54}Mn. It is confirmed that the induced activity in SS316 and F82H can be evaluated with 14 % accuracy although further consideration is needed for the activity of ^{54}Mn in F82H.

4. Summary

Cross section data of deuteron-induced reactions for pure metals used as IFMIF accelerator structural materials were measured within the accuracy of 10~20 %. TALYS is closer to the present data than ACSELAM for most reactions.

We have measured and evaluated activity of each nuclide induced by deuteron of 39.5 MeV in SS316 and F82H. As the result of the comparison between the measured and evaluated activities, it is confirmed that the induced activity in SS316 and F82H could be evaluated with 14 % accuracy except for ^{54}Mn in F82H.

Acknowledgements

The authors would like to express their thanks to AVF cyclotron staffs of the TIARA facility, JAEA for operating the accelerator steadily.

References

1) IFMIF International Team : "IFMIF-KEP International Fusion Materials Irradiation Facility key element technology phase report" , JAERI-Tech 2003-005 (2003).
2) S. Tanaka, M. Fukuda and K. Nishimura : "IRACM: A Code System to Calculate Induced Radioactivity Produced by Ions and Neutrons" , JAERI-Data/Code 97-019 (1997).
3) S. Takacs, F. Szelecsenyi., F. Tarkanyi, M. Sonck, A. Hermanne, Y. Shubin, A. Dityuk, M.G. Mustafa and Z. Youxizng : "New cross-sections and intercomparison of deuteron monitor reactions on Al, Ti, Fe, Ni and Cu" , Nucl. Inst. Meth. B174, 235 (2001).
4) T. Fukahori : "Proc. The Specialists' Meeting on High Energy Nuclear Data" , JAERI-M 92-039, 114 (1992).
5) A. J. Koning, S. Hilaire and M. Duijvestijn : "TALYS-0.64 A nuclear reaction program USER MANUAL" , NRG Report 21297/04.62741/P (2004).
6) U. Martens and G. W. Schweimer : "Production of be-7, Na-22, Na-24 and Mg-28 by irradiation of Al-27 with 52 MeV deuterons and 104 MeV alpha particles" , Zeitschrift fur Physik, 233, 170 (1970).
7) R. Michel, G. Brinkmann, M. Galas and R. Stuck : EXFOR No. A0158, (1982).
8) R. L. Wilson, D. J. Frantsvog, A. R. Kunselman, C. Detraz and C. S. Zaidins : "Excitation functions of reactions induced by ^{1}H and ^{2}H ions on natural Mg, Al and Si" , Phys. Rev. C13, 976 (1976).
9) R.Weinreich, H. J. Probst and S. M. Qaim : " Production of chromium-48 for applications in life science" , Int. J. Appl. Radiat. Isot. 31, 223 (1980).
10) J. W. Clark, C. B. Fulmer and I. R. Williams : "Excitation function for radioactive nuclides produced by deuteron-induced reactions in iron" , Phys. Rev. 179, 1104 (1969).
11) A. Hermanne, M. Sonck, S. Takacs and F. Tarkanyi : "Experimental study of excitation function for some reactions induced by deuteron (10-50 MeV) on natural Fe and Ti" , Nucl. Inst. Meth. B161-163, 178 (2000).
12) C. K. Cline : "Reaction mechanisms and shell structure effects in ^{54}Fe+^{6}Li and ^{58}Ni+d reactions at medium energies" , Nucl. Phys. A174, 73 (1971).
13) F. O. Bartell, A. C. Helmholz, S. D. Softky and D. B. Stewart : "Excitation functions for spallation reactions on Cu" , Phys. Rev. 80, 1006 (1950).
14) C. B. Fulmer and I. R. Williams **:** "Excitation functions for radioactive nucleides produced by deuteron-induced reactions in copper" , Nucl. Phys. A155, 40 (1970).
15) J. Bisplinghoff, J. Ernst, T. Mayer-kuckuk, P. Jahn and C. Mayer-Boricke **:** "Analysis of (particle, *x*n) reactions on tantalum and gold : (III). Excitation functions of d-induced reactions on ^{181}Ta from 10 to 80 MeV and equilibrium statistical analysis" **,** Nucl. Phys. A228-1, 180 (1974).
16) F. Tarkanyi, S. Takacs, F. Szelecsenyi, F. Ditroi, A. Hermanne and M. Sonck : "Excitation functions of deuteron induced nuclear reactions on natural tungsten up to 50 MeV" , Nucl. Inst. Meth. B211, 319 (2003).

Table 1 Purity and thickness for pure metal foils

	atomic weight (g/mol)	purity (%)	thickness (μm)	isotope ratio (%)
Al	26.981538	99.99	200	^{27}Al(100)
V	50.9415	99.8	25	^{50}V(0.250), ^{51}V(99.750)
Cr	51.9961	99.99	25	^{50}Cr(4.345), ^{52}Cr(83.789), ^{53}Cr(9.501), ^{54}Cr(2.365)
Mn	54.938049	99	25	55Mn(100)
Fe	55.845	99.95	50	^{54}Fe(5.845), ^{56}Fe(91.754), ^{57}Fe(2.119), ^{58}Fe(0.282)
Ni	58.6934	99	20	^{58}Ni(68.0769), ^{60}Ni(26.2231), ^{61}Ni(1.1399), ^{62}Ni(3.6345), ^{64}Ni(0.9256)
Cu	63.546	99.99	25	^{63}Cu(69.17), ^{65}Cu(30.83)
Ta	180.9479	99.95	10	^{180}Ta(0.012), ^{181}Ta(99.988)
W	183.84	99.95	20	^{180}W(0.12), ^{182}W(26.50), ^{183}W(14.31), ^{184}W(30.64), ^{186}W(28.43)
Au	196.96655	99.95	30	^{197}Au(100)

Table 2 Composition and density for alloy foils

element	SS316	F82H
	(wt%)	
V	—	0.18
Cr	17.2	7.74
Mn	1.58	0.10
Fe	65.5	89.74
Ni	12.4	<0.02
Mo	2.07	<0.01
Ta	—	0.04
W	<0.03	1.95
density (g/cm^3)	6.96	7.60

Table 3 Cross section for the $^{nat}Cr(d,x)^{48}V$, ^{52}Mn, $^{55}Mn(d,x)^{54}Mn$ and $^{nat}Ni(d,x)^{56}Co$ reactions

reaction	cross section (mb)			ratio	
(E_d= 39.5 MeV)	present (error)	ACSELAM	TALYS	ACS/present	TAL/present
$^{nat}Cr(d,x)^{48}V$	69.3 (9.8)	38.2	47.9	0.55	0.69
$^{nat}Cr(d,x)^{52}Mn$	48.0 (6.6)	111.9	68.2	2.33	1.42
$^{55}Mn(d,x)^{54}Mn$	507.4 (68.6)	201.2	342.5	0.40	0.68
$^{nat}Ni(d,x)^{56}Co$	88.4 (11.9)	93.2	146.2	1.05	1.65

Table 4 Deuteron induced activity of nuclides produced in SS316 and F82H

product	target	SS316			F82H		
		meas. (kBq/cm^3)	eval. (kBq/cm^3)	eval./meas.	meas. (kBq/cm^3)	eval. (kBq/cm^3)	eval./meas.
^{48}V	^{nat}Cr	46.2	47.1	1.02	20.7	21.9	1.06
^{52}Mn	^{nat}Cr, ^{nat}Fe	500.4	515.4	1.03	585.8	630.9	1.08
^{54}Mn	^{55}Mn, ^{nat}Fe	13.7	14.5	1.06	14.3	18.5	1.29
^{56}Co	^{nat}Fe, ^{nat}Ni	40.0	42.0	1.05	42.9	48.0	1.12
^{57}Co	^{nat}Fe, ^{nat}Ni	17.8	17.4	0.98	5.4	5.6	1.04
^{181}Re	^{nat}W	—	—	—	213.0	229.2	1.08

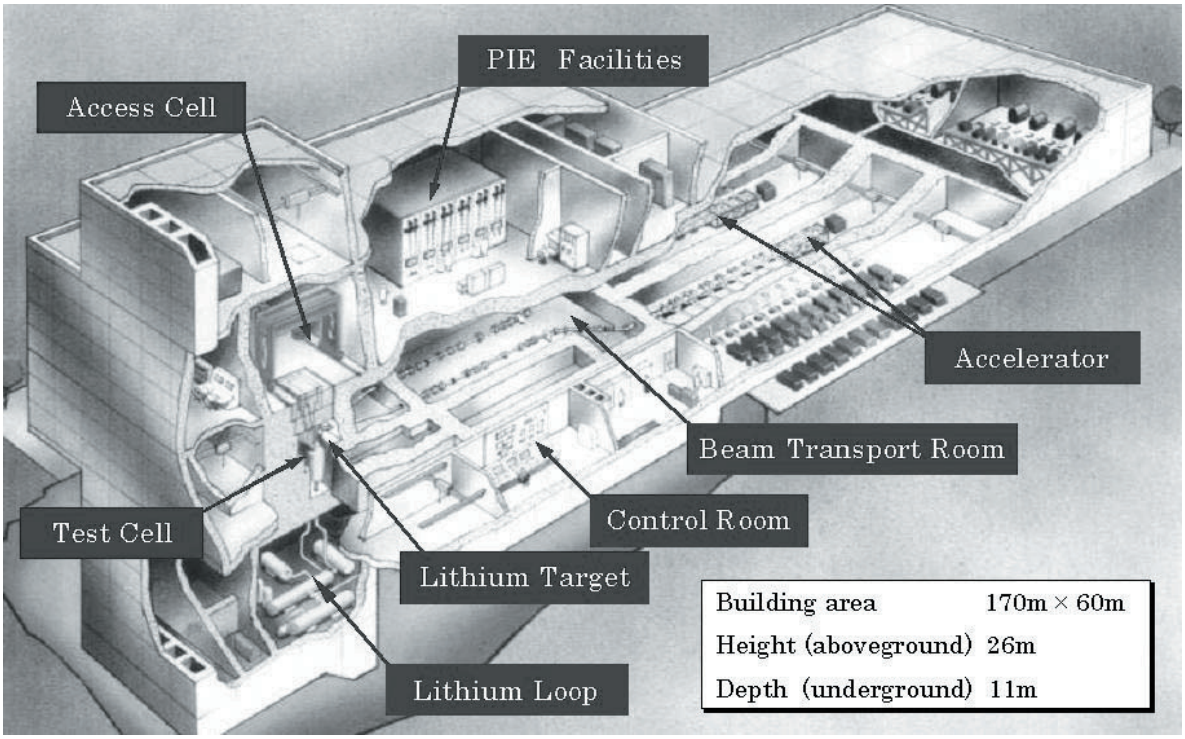

Fig. 1 IFMIF bird view

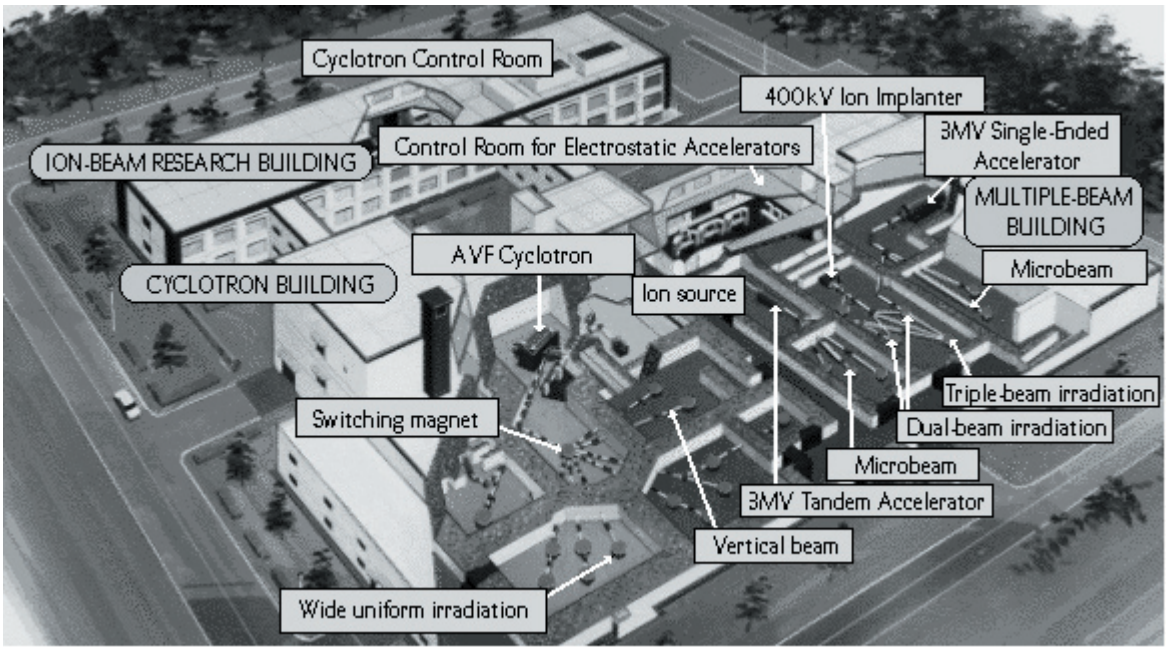

Fig. 2 TIARA bird view

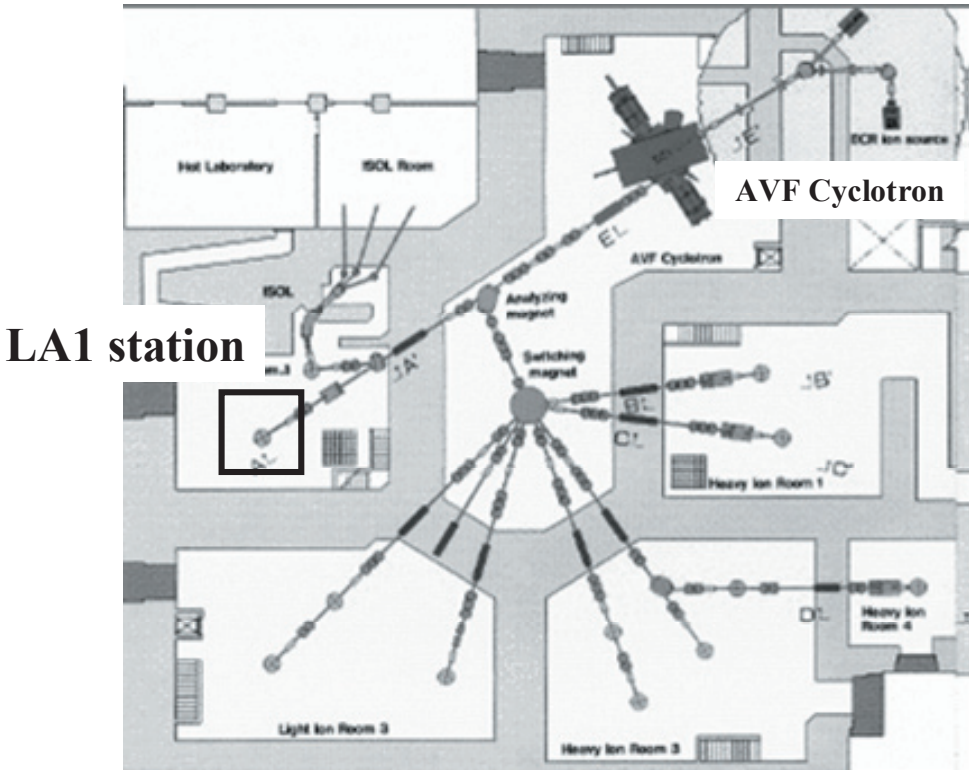

Fig. 3 TIARA beam transport lines

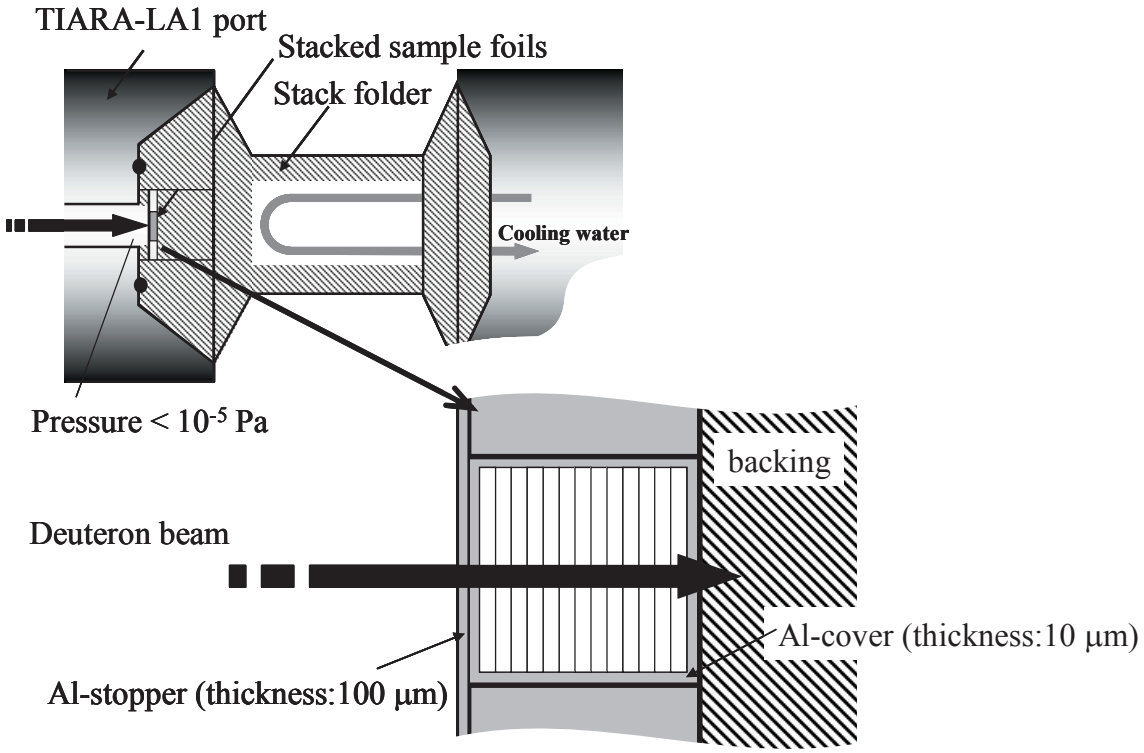

Fig. 4 schematic view of a stack folder

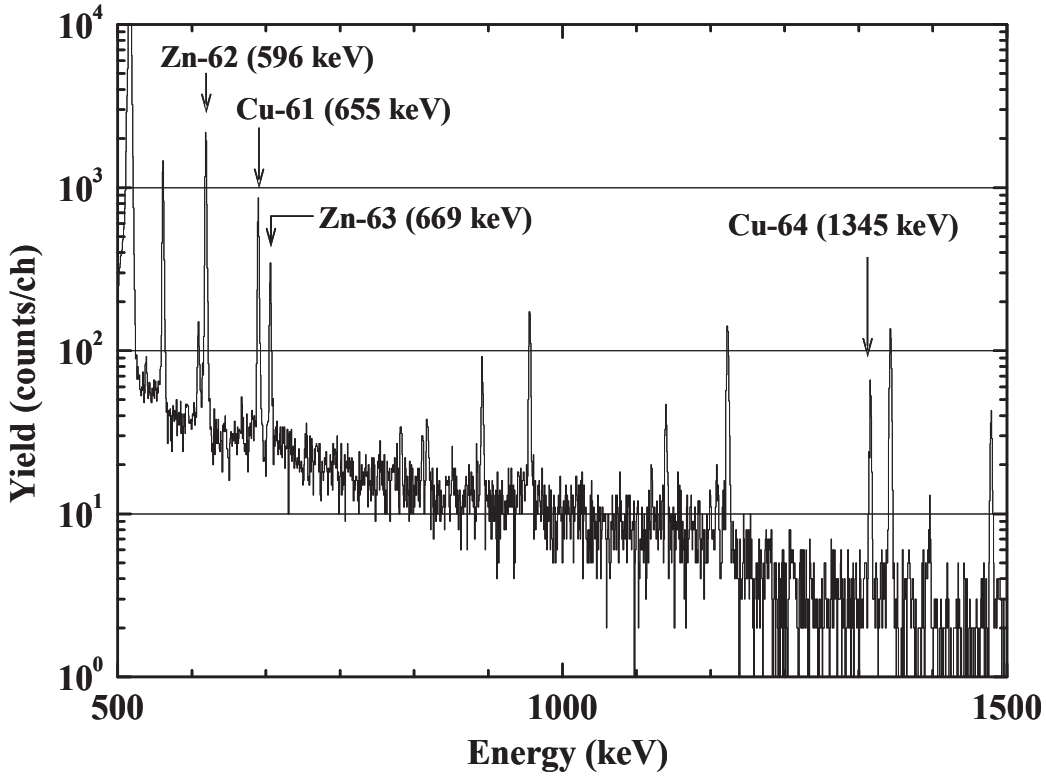

Fig. 5 Typical gamma-ray spectrum from Cu foil

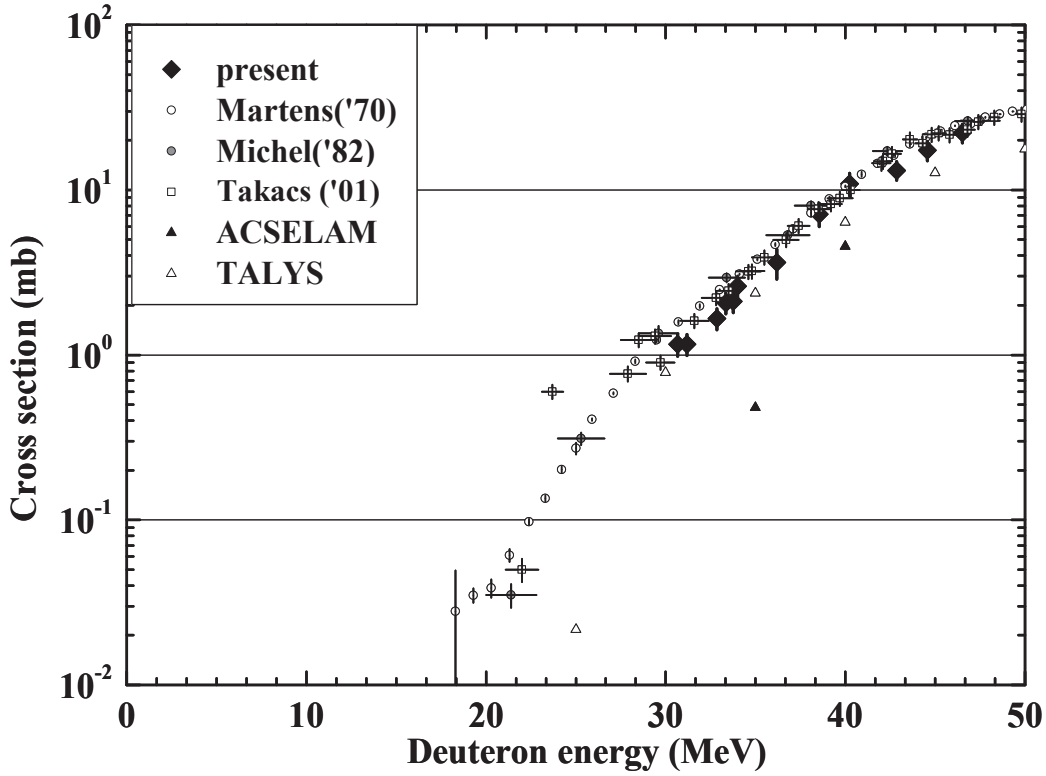

Fig. 6 Cross section for the $^{27}Al(d,x)^{22}Na$ reaction

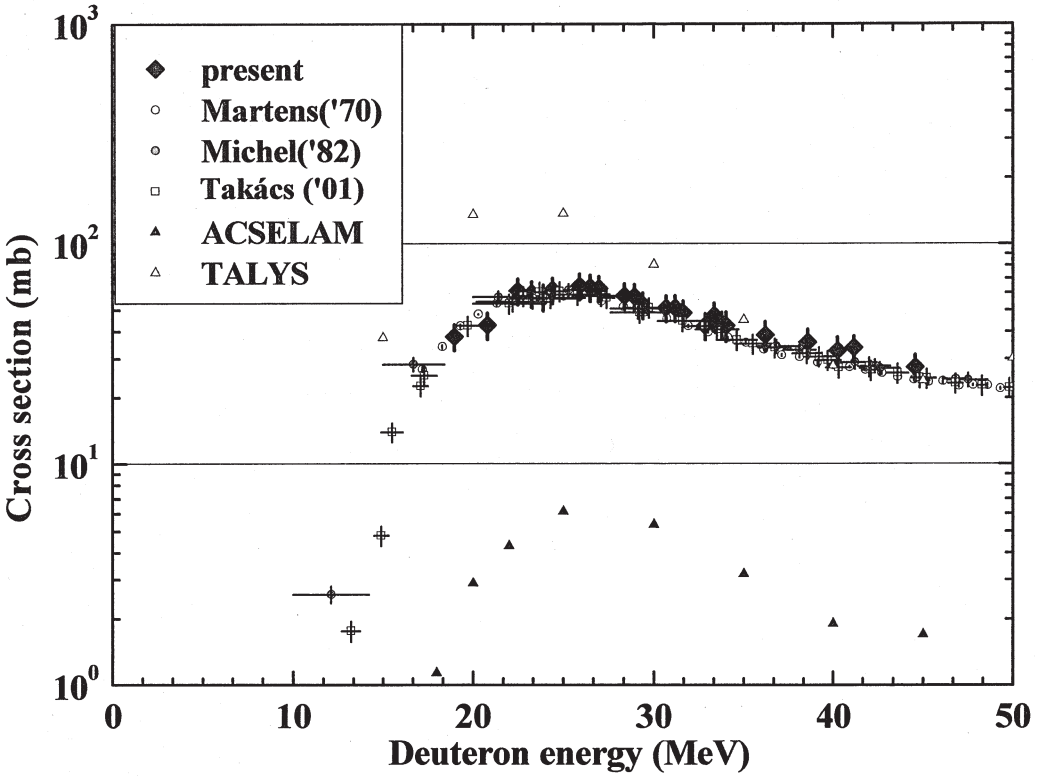

Fig. 7 Cross section for the $^{27}Al(d,x)^{24}Na$ reaction

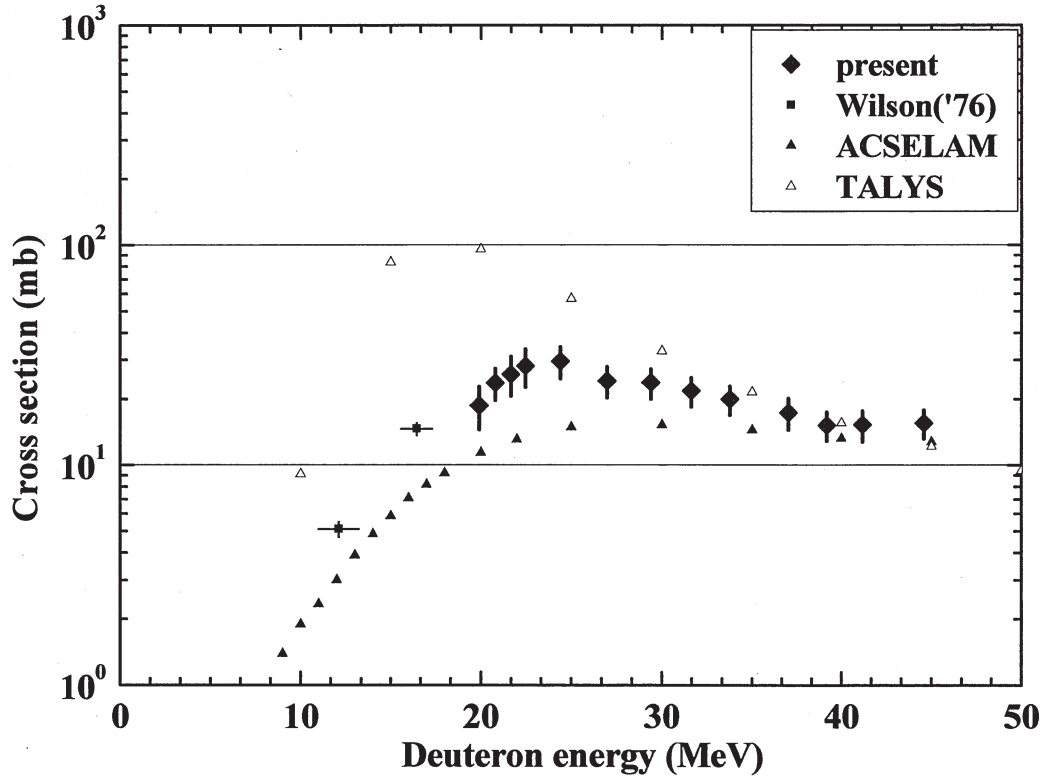

Fig. 8 Cross section for the $^{27}Al(d,2p)^{27}Mg$ reaction

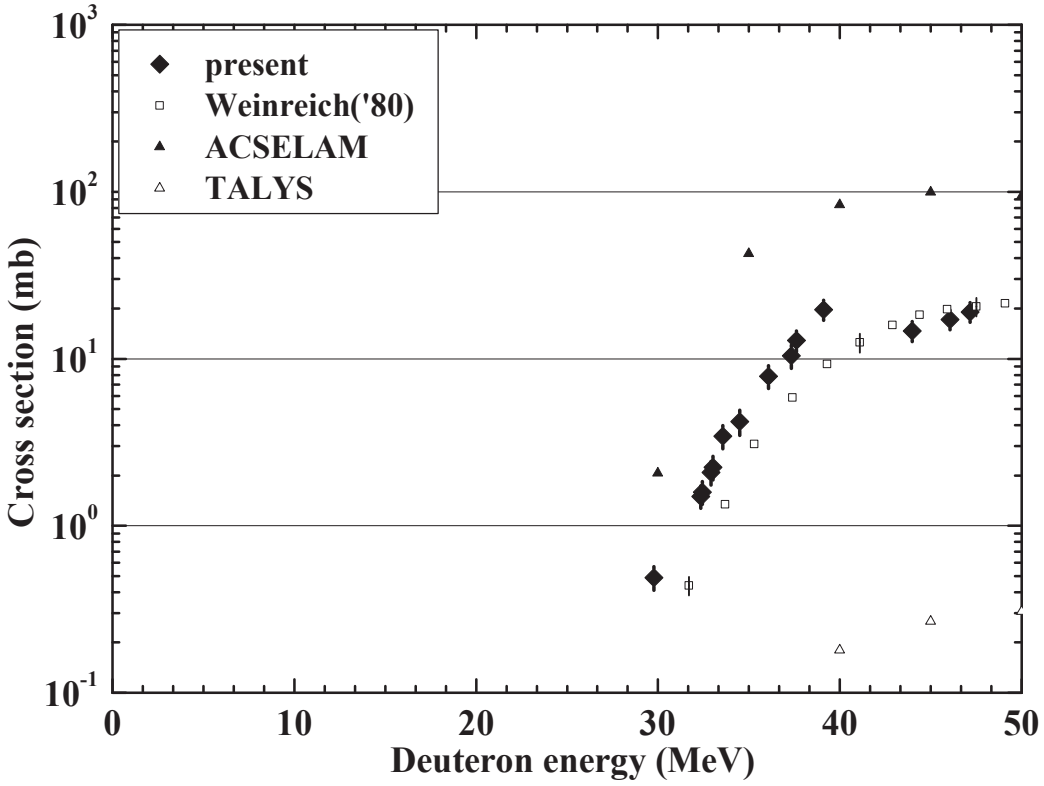

Fig. 9 Cross section for the $^{51}V(d,4n)^{49}Cr$ reaction

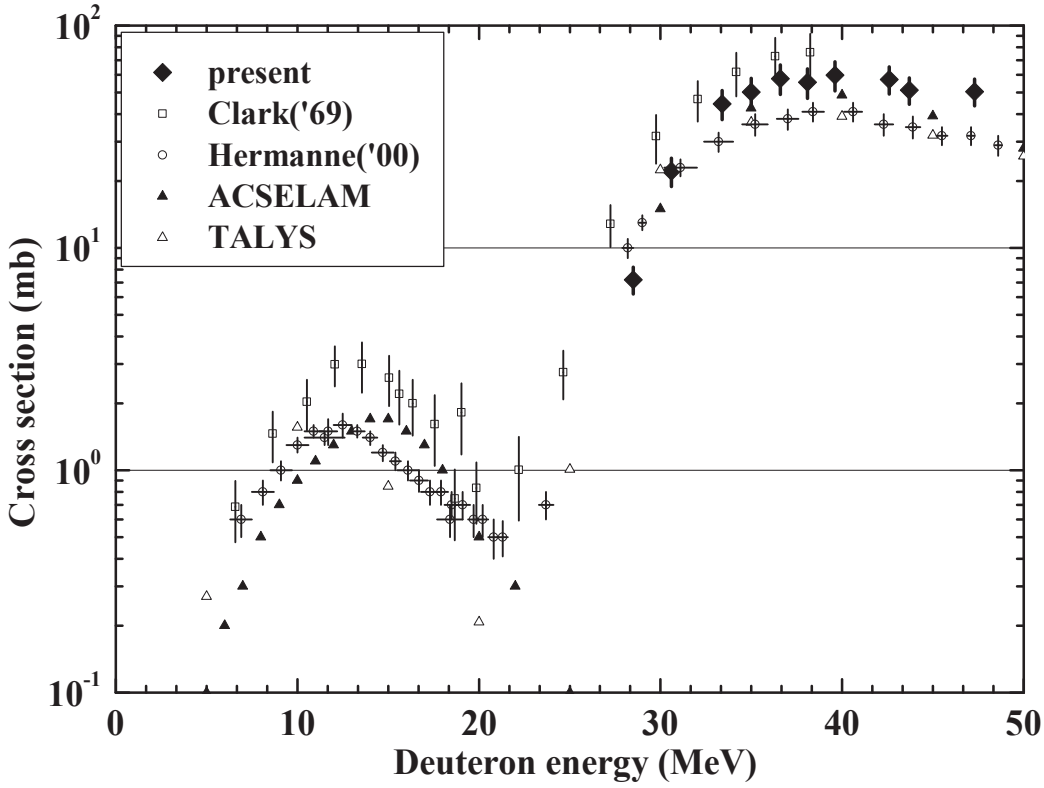

Fig. 10 Cross section for the $^{nat}Fe(d,x)^{52}Mn$ reaction

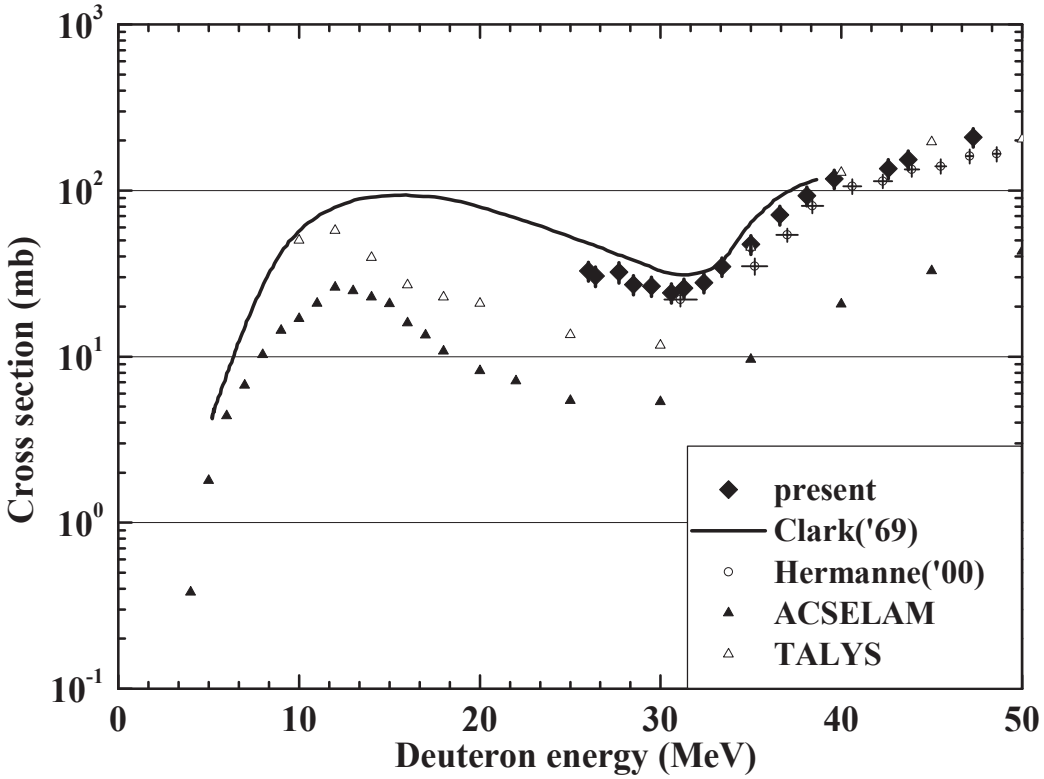

Fig. 11 Cross section for the $^{nat}Fe(d,x)^{54}Mn$ reaction

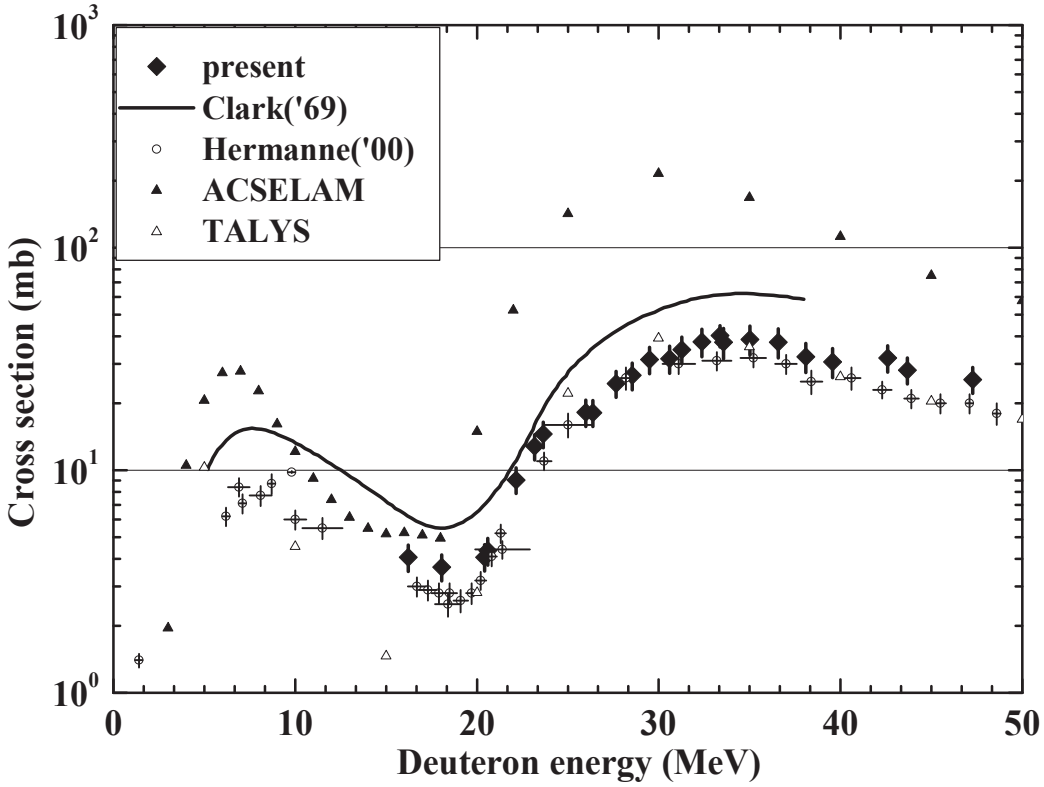

Fig. 12 Cross section for the $^{nat}Fe(d,x)^{55}Co$ reaction

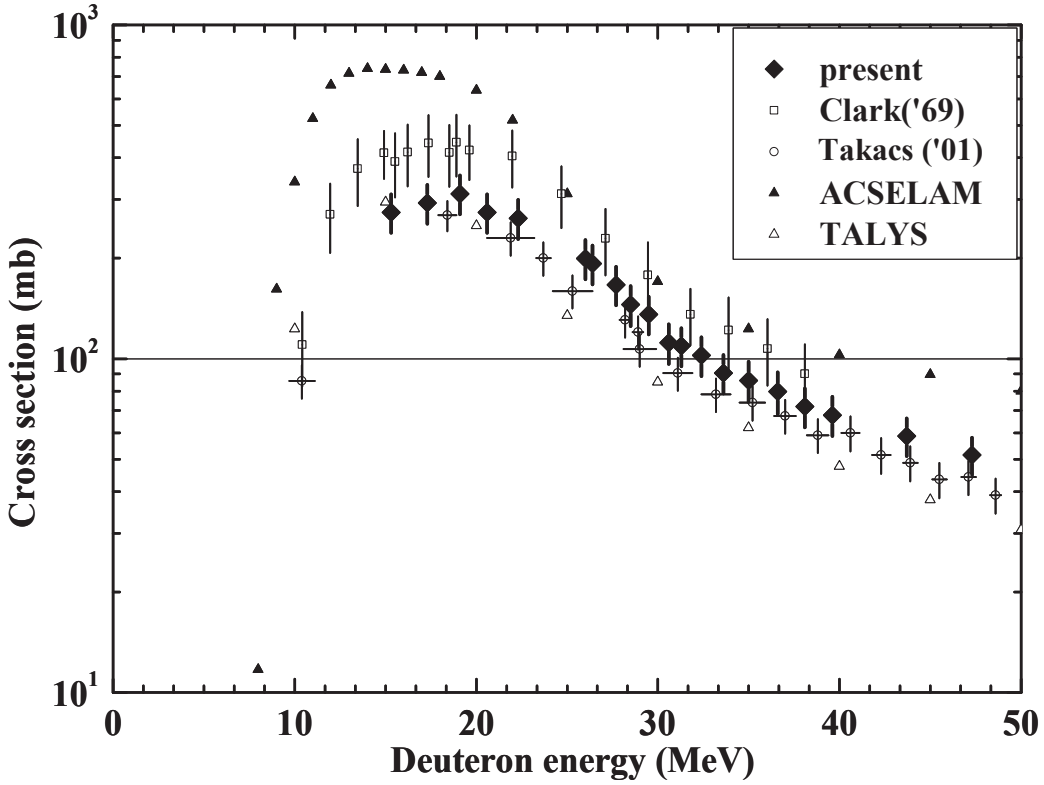

Fig. 13 Cross section for the $^{nat}Fe(d,x)^{56}Co$ reaction

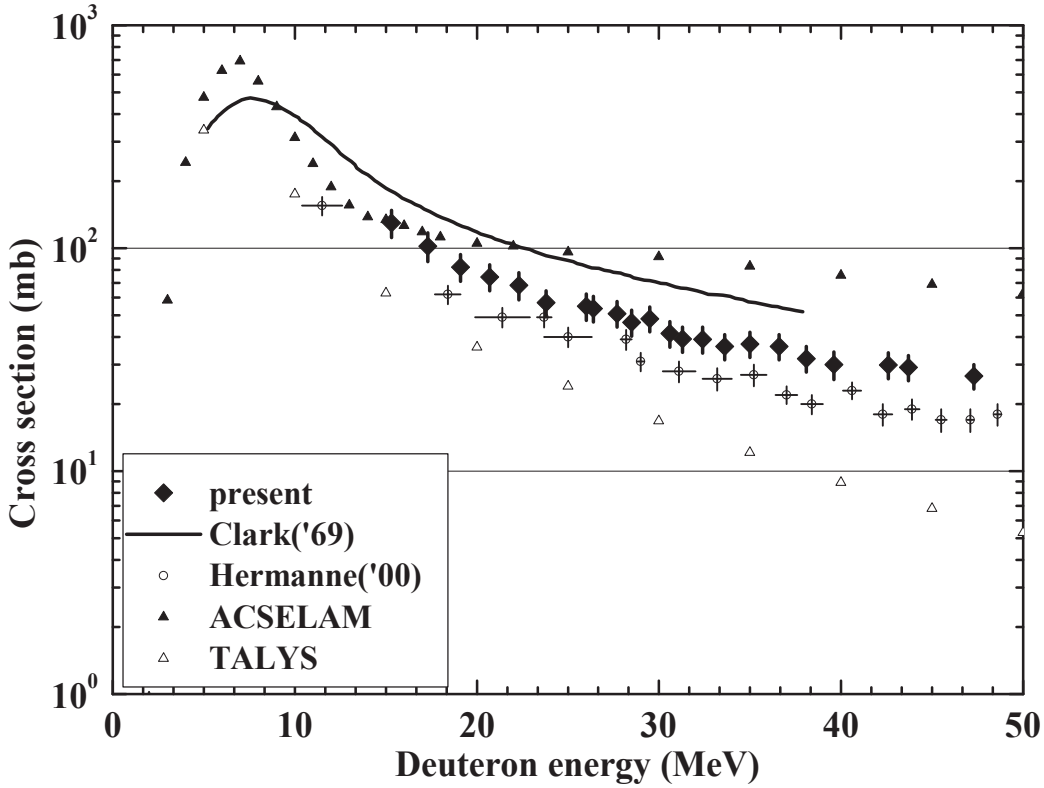

Fig. 14 Cross section for the $^{nat}Fe(d,x)^{57}Co$ reaction

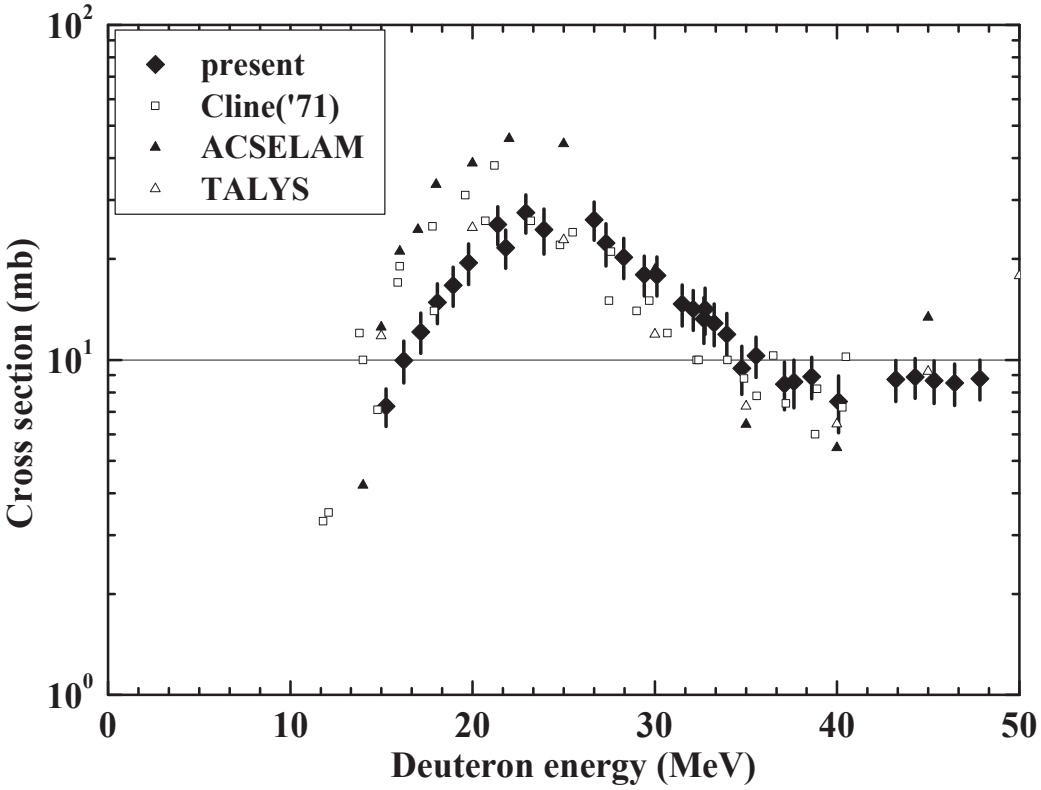

Fig. 15 Cross section for the $^{nat}Ni(d,x)^{55}Co$ reaction

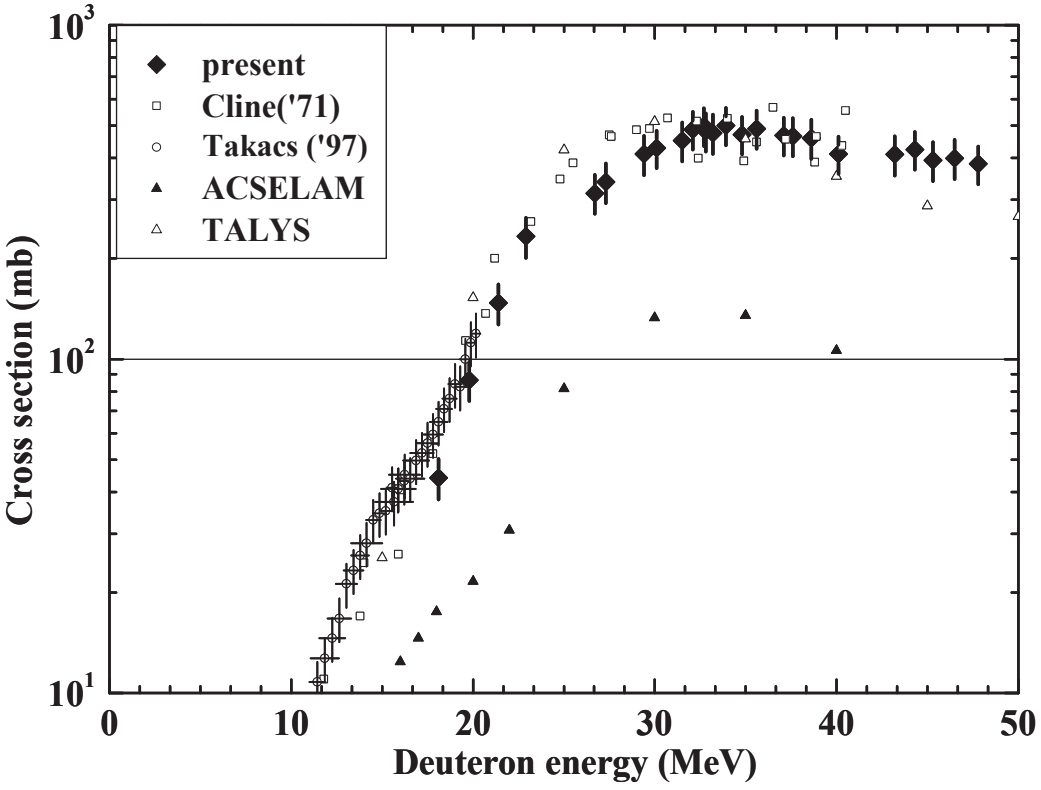

Fig. 16 Cross section for the $^{nat}Ni(d,x)^{57}Co$ reaction

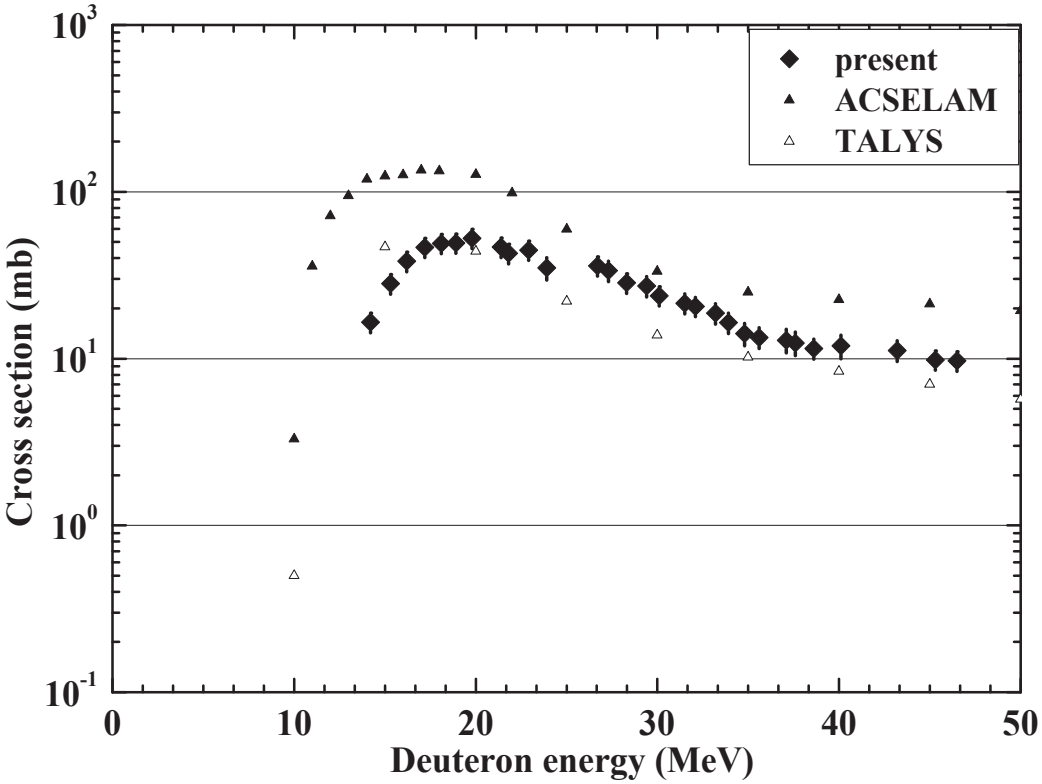

Fig. 17 Cross section for the $^{nat}Ni(d,x)^{60}Cu$ reaction

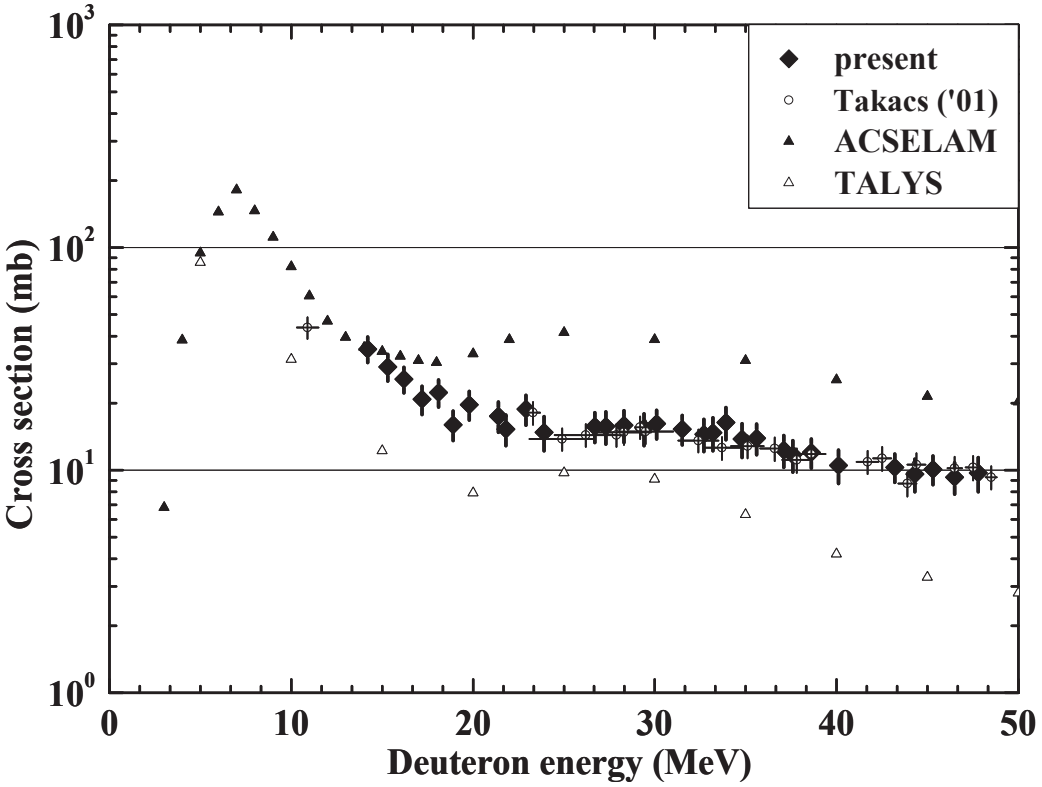

Fig. 18 Cross section for the $^{nat}Ni(d,x)^{61}Cu$ reaction

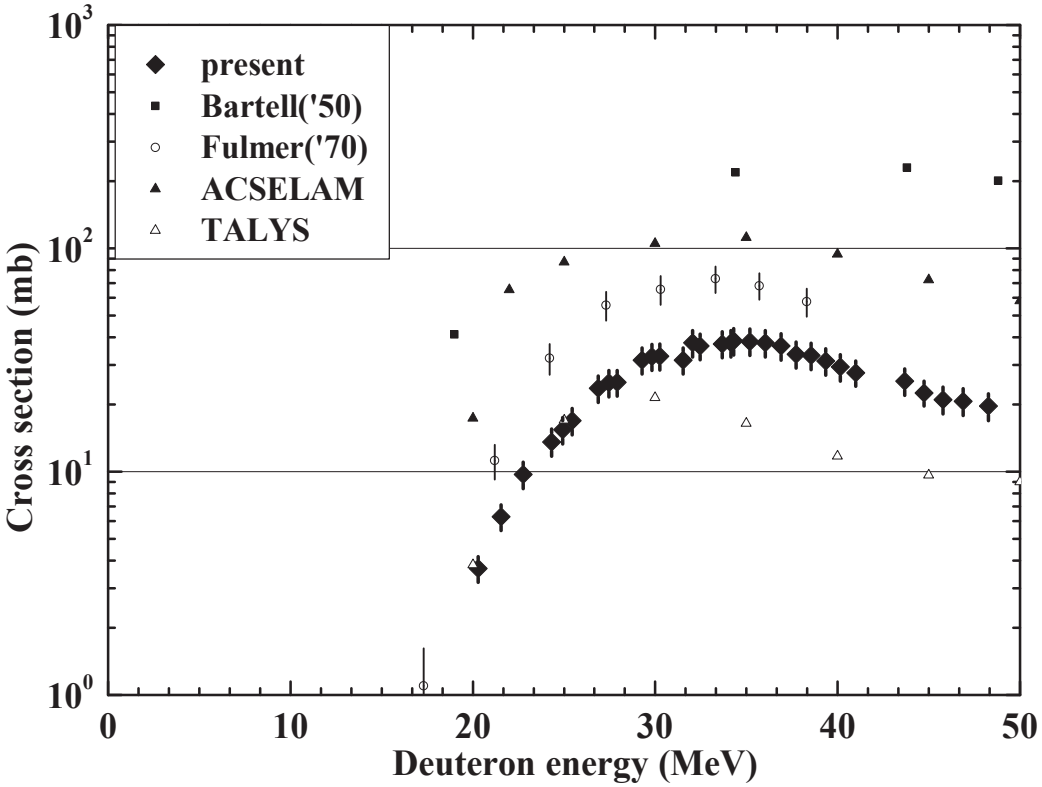

Fig. 19 Cross section for the $^{nat}Cu(d,x)^{62}Zn$ reaction

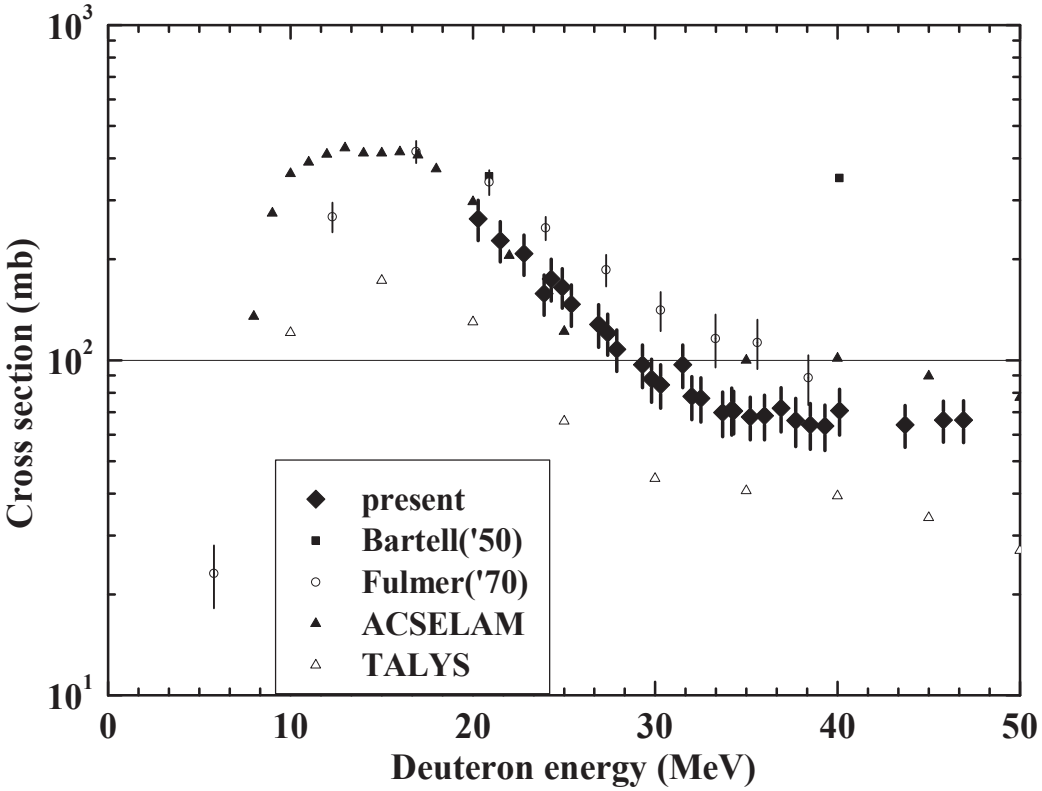

Fig. 20 Cross section for the $^{nat}Cu(d,x)^{63}Zn$ reaction

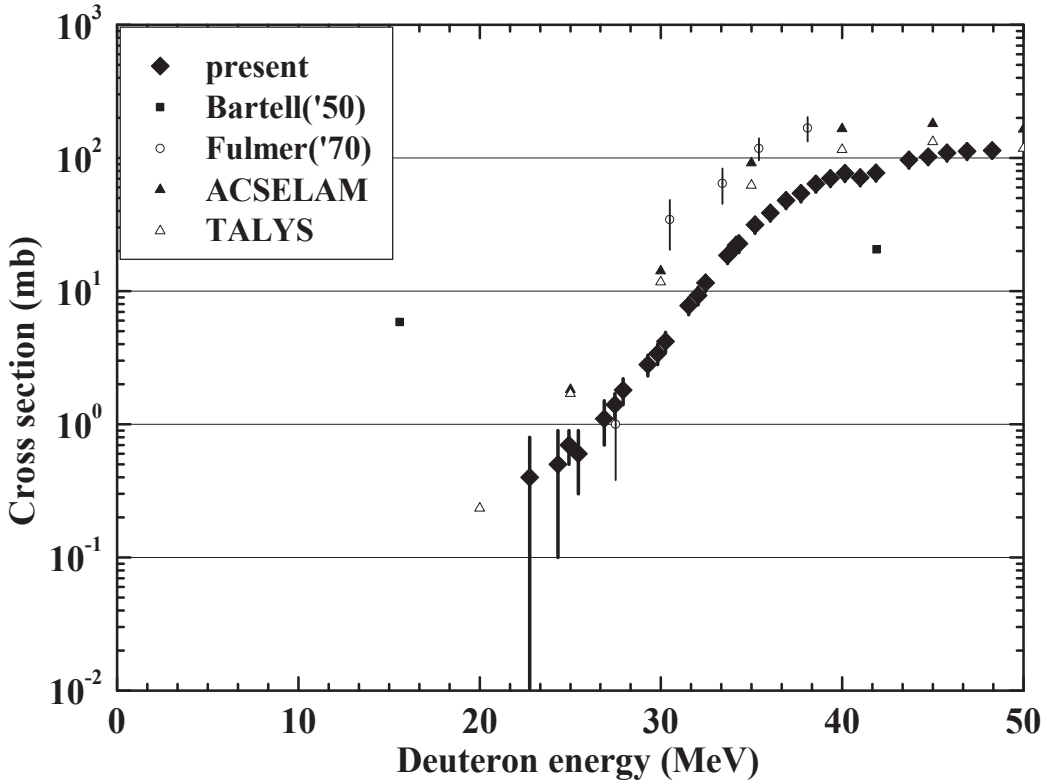

Fig. 21 Cross section for the $^{nat}Cu(d,x)^{61}Cu$ reaction

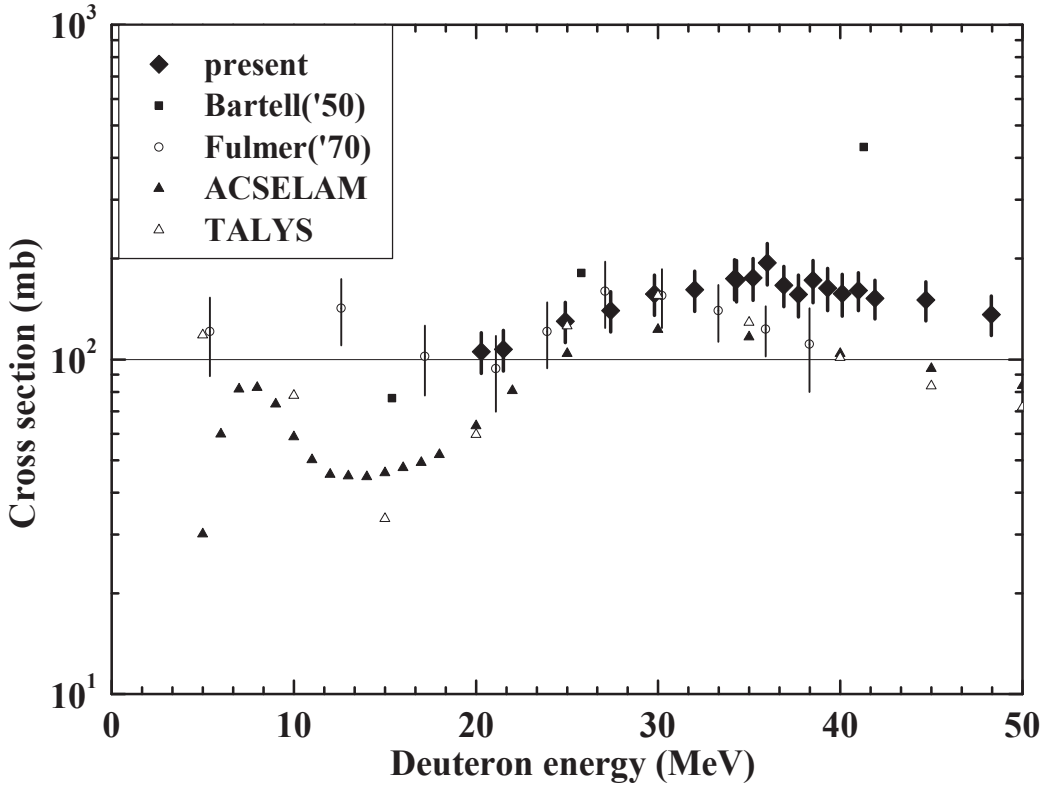

Fig. 22 Cross section for the $^{nat}Cu(d,x)^{64}Cu$ reaction

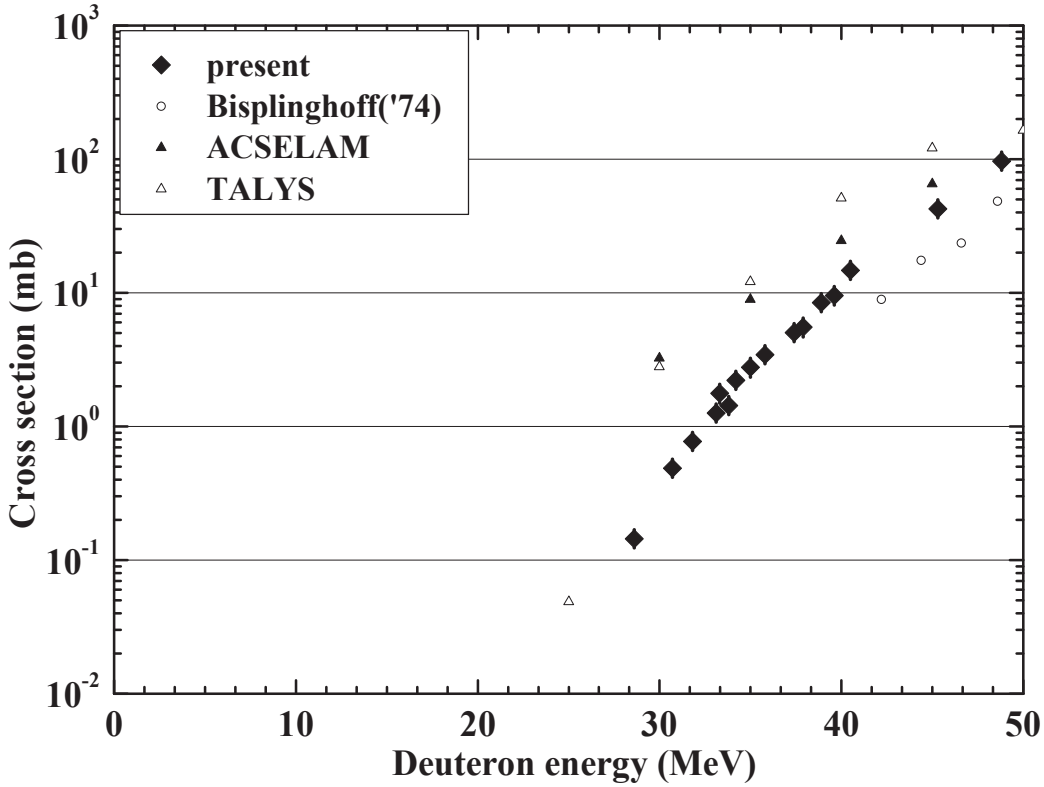

Fig. 23 Cross section for the ^{nat}Ta(d,x)^{178}Ta reaction

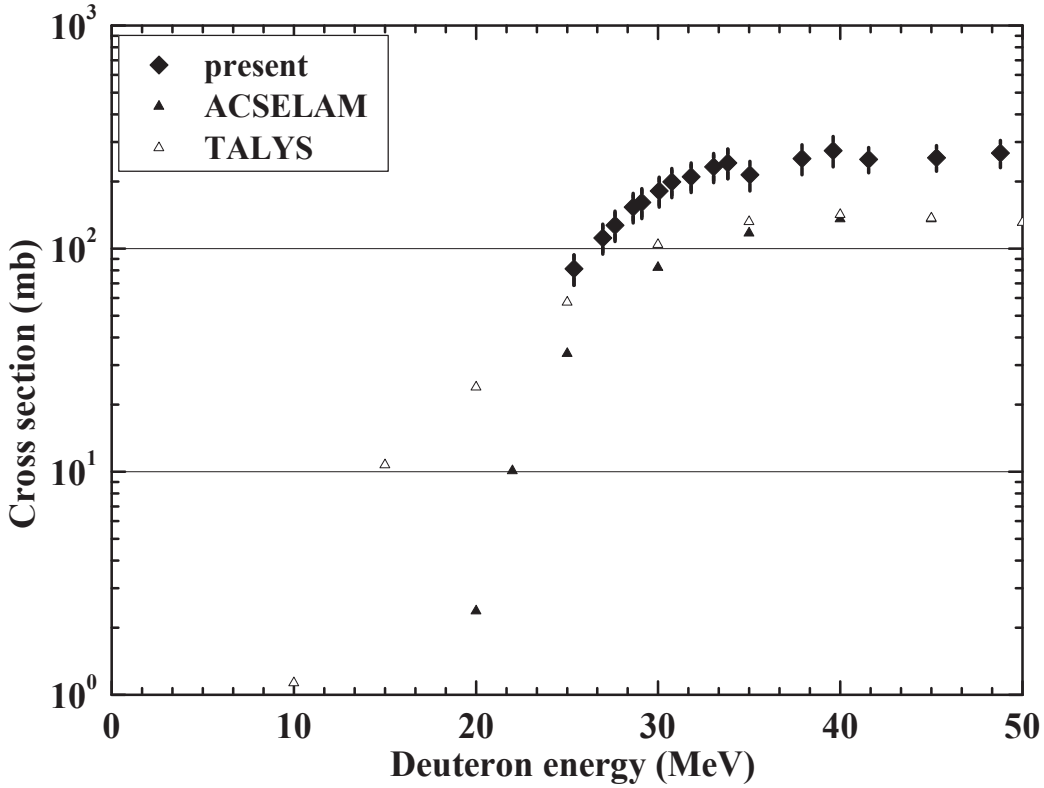

Fig. 24 Cross section for the ^{nat}Ta(d,x)^{180}Ta reaction

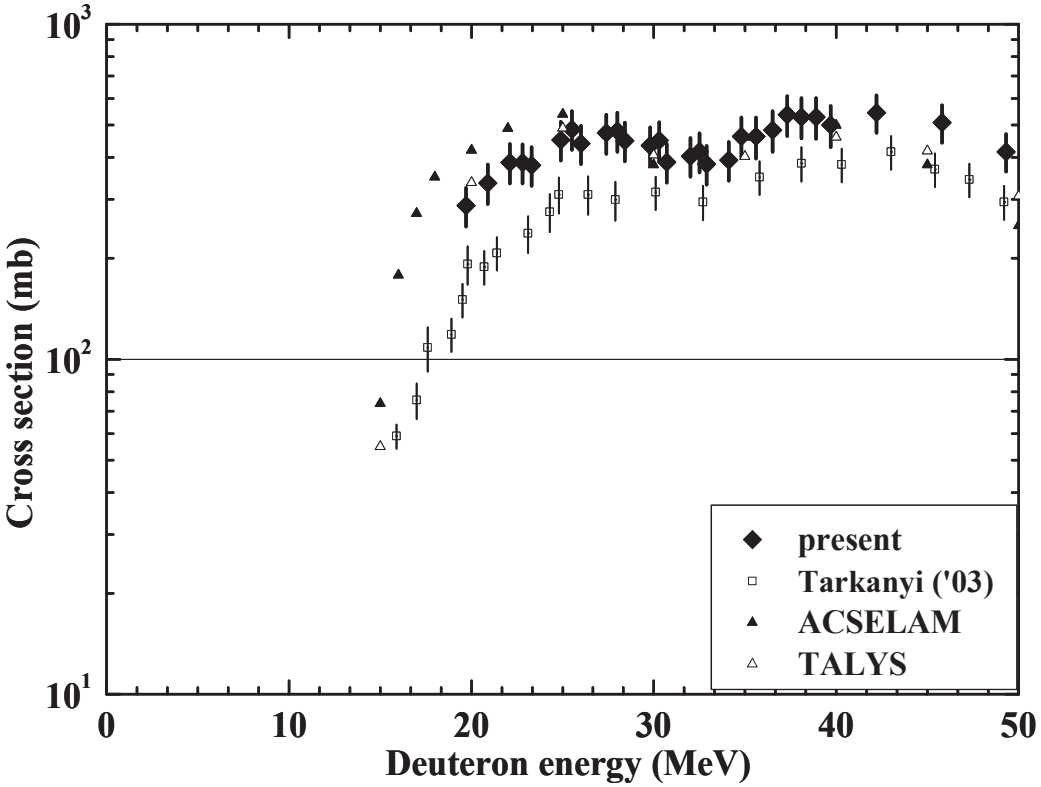

Fig. 25 Cross section for the $^{nat}W(d,x)^{181}Re$ reaction

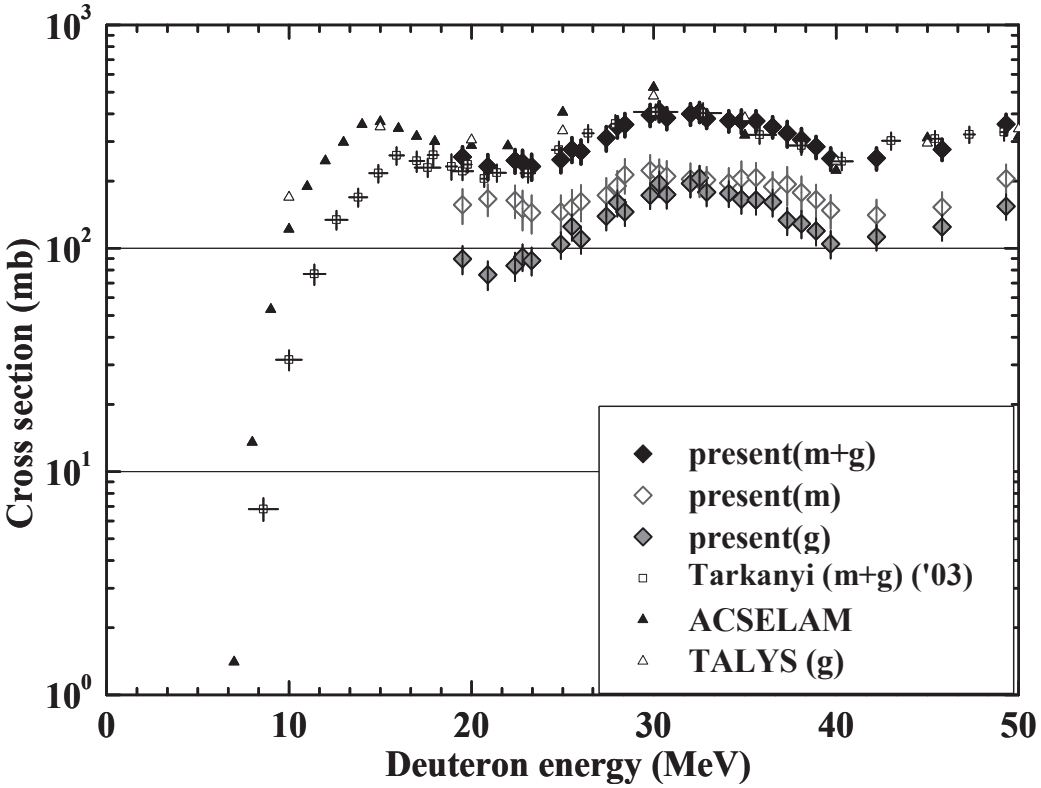

Fig. 26 Cross section for the $^{nat}W(d,x)^{182}Re$ reaction

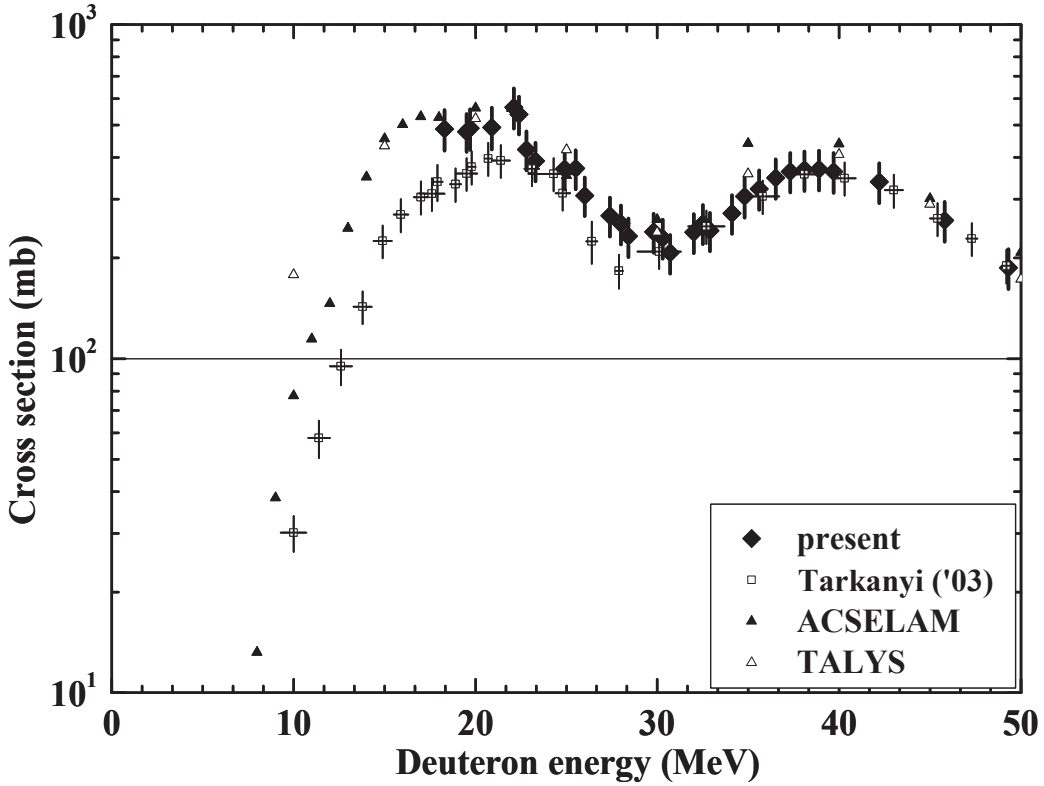

Fig. 27 Cross section for the $^{nat}W(d,x)^{183}Re$ reaction

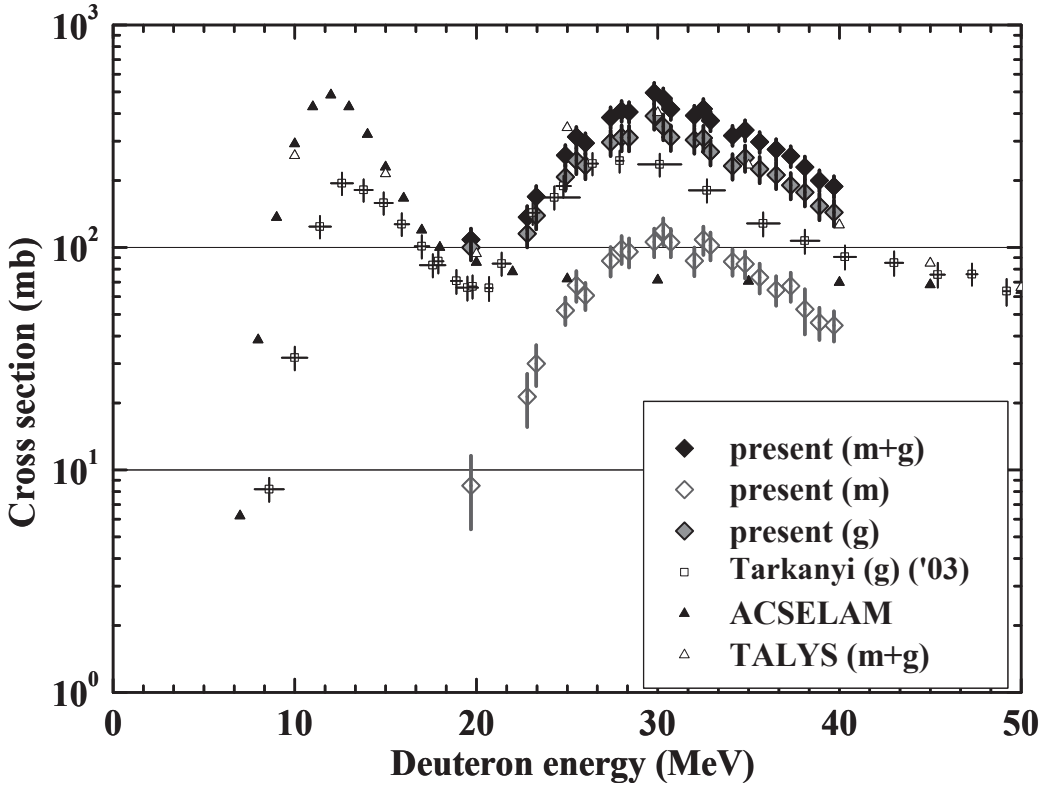

Fig. 28 Cross section for the $^{nat}W(d,x)^{184}Re$ reaction

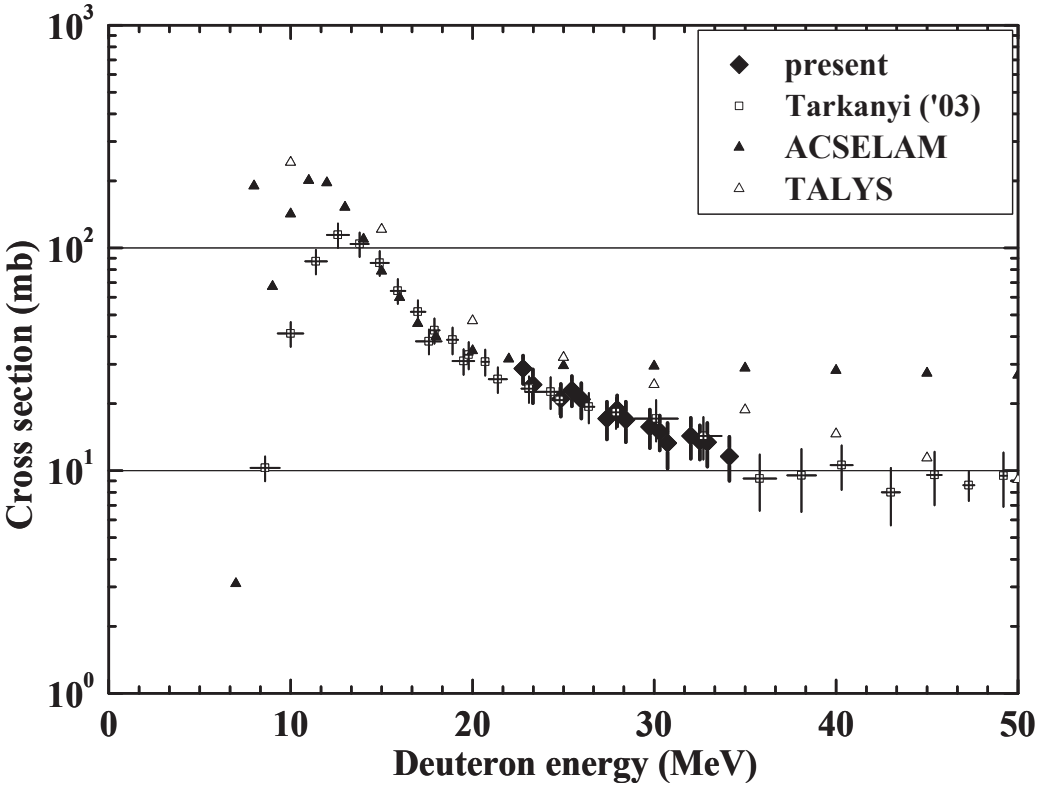

Fig. 29 Cross section for the $^{nat}W(d,x)^{186}Re$ reaction

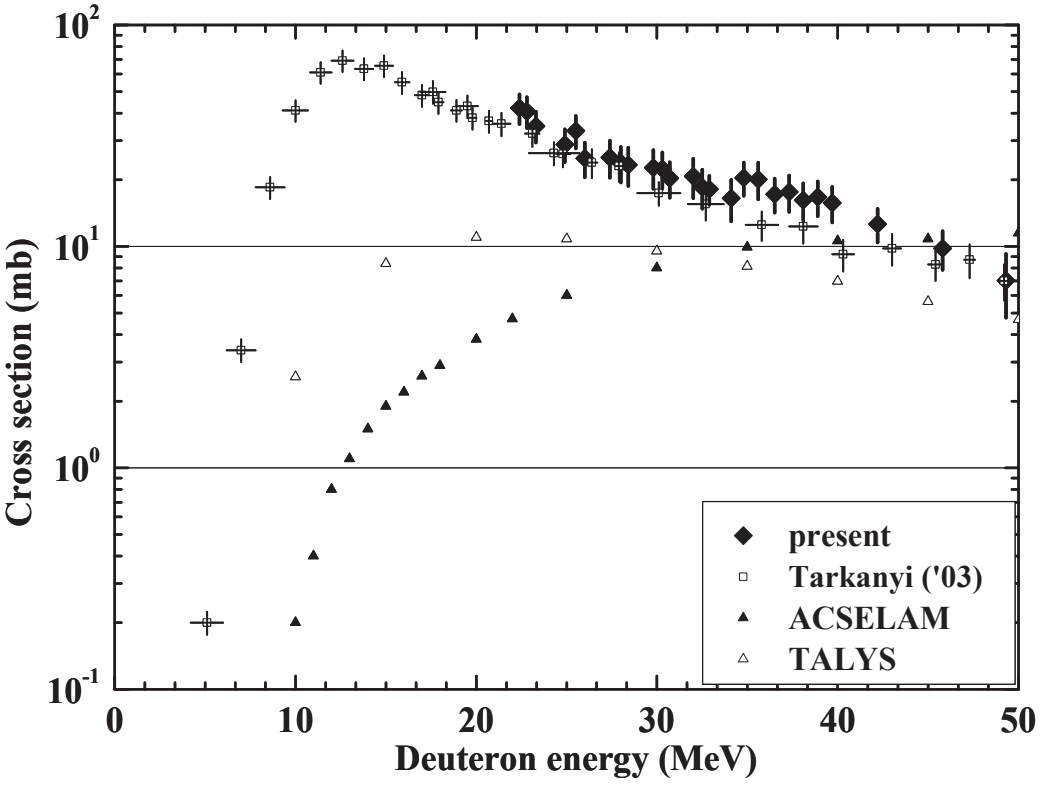

Fig. 30 Cross section for the $^{nat}W(d,x)^{187}W$ reaction

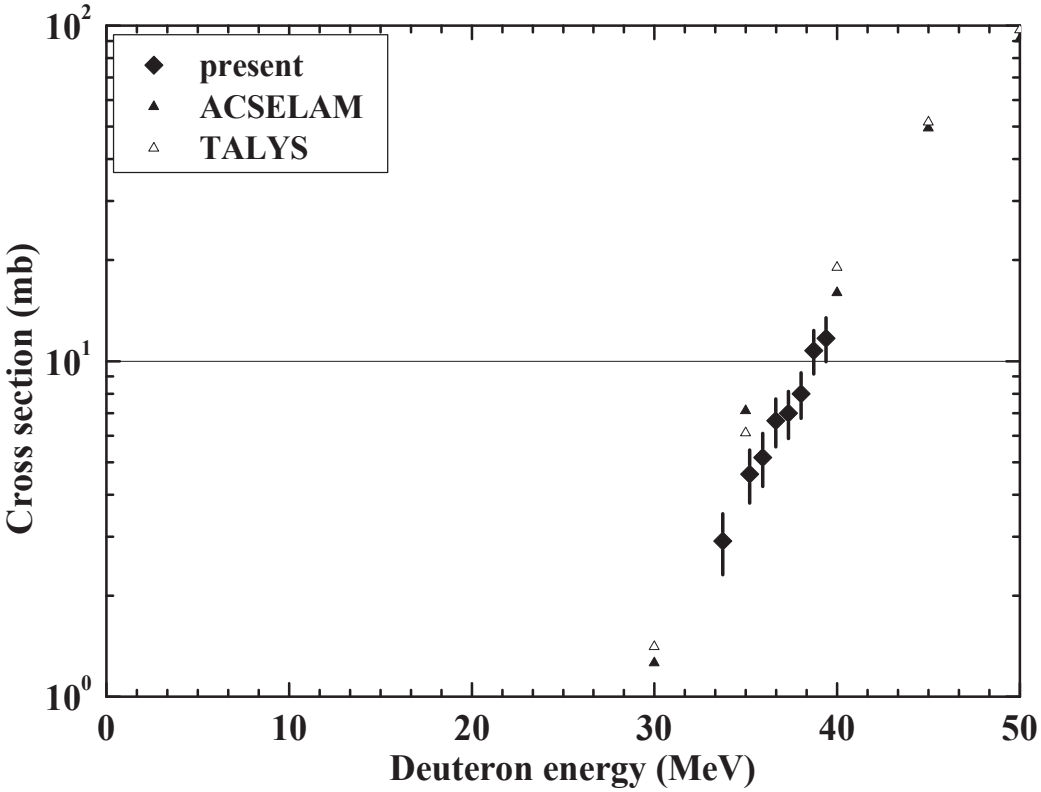

Fig. 31 Cross section for the ^{197}Au(d,x) ^{194}Au reaction

Appendix - Numerical values of activation cross sections

Table A-1 Measured cross section of the ^{27}Al + d reactions

^{27}Al(d,2p)^{27}Mg			^{27}Al(d,x)^{22}Na			^{27}Al(d,x)^{24}Na		
E_d (MeV)	σ (mb)	$\Delta\sigma$ (mb)	E_d (MeV)	σ (mb)	$\Delta\sigma$ (mb)	E_d (MeV)	σ (mb)	$\Delta\sigma$ (mb)
9.89	18.66	4.13	30.67	1.16	0.18	18.96	37.77	5.08
20.78	23.61	3.85	31.19	1.16	0.17	20.78	42.62	5.82
21.65	25.87	5.29	32.86	1.66	0.24	22.48	61.09	8.34
22.48	28.16	5.56	33.35	2.11	0.30	23.25	59.30	8.00
24.41	29.60	4.90	33.76	2.07	0.31	23.88	57.10	7.70
26.97	24.10	3.90	33.99	2.61	0.40	24.41	61.60	8.20
29.36	23.70	3.70	36.18	3.63	0.75	25.90	64.10	8.60
31.62	21.70	3.30	38.54	7.14	1.14	26.48	63.30	8.50
33.76	19.90	3.00	40.23	10.91	1.69	26.97	62.70	8.30
37.01	17.32	2.83	42.86	13.12	1.69	28.36	58.00	7.80
39.18	15.17	2.32	44.57	17.34	2.32	28.91	57.40	7.70
41.17	15.25	2.46	46.51	22.19	2.89	29.36	52.60	7.00
44.57	15.51	2.31				30.67	51.10	6.90
						31.19	51.10	6.90
						31.62	48.50	6.50
						32.86	42.40	5.70
						33.35	47.10	6.40
						33.76	43.00	5.70
						33.99	42.39	6.42
						36.18	38.43	5.82
						38.54	35.59	5.40
						40.23	32.61	4.94
						41.17	33.62	4.45
						44.57	27.53	3.77

Table A-2 Measured cross section of the ^{51}V + d reaction

$^{51}V(d,4n)^{49}Cr$		
E_d (MeV)	σ (mb)	$\Delta\sigma$ (mb)
29.77	0.49	0.08
32.36	1.50	0.23
32.43	1.59	0.25
32.92	2.09	0.34
33.02	2.24	0.36
33.57	3.44	0.55
34.49	4.20	0.72
36.08	7.87	1.24
37.33	10.41	1.67
37.61	12.84	1.84
39.10	19.69	2.72
43.97	14.69	2.00
46.06	17.20	2.32
47.16	19.08	2.57

Table A-3 Measured cross section of the ^{nat}Fe + d reactions

^{nat}Fe(d,x) ^{52}Mn			^{nat}Fe(d,x)^{54}Mn			^{nat}Fe(d,x)^{55}Co		
E_d (MeV)	σ (mb)	$\Delta\sigma$ (mb)	E_d (MeV)	σ (mb)	$\Delta\sigma$ (mb)	E_d (MeV)	σ (mb)	$\Delta\sigma$ (mb)
28.54	7.18	1.02	25.98	32.68	4.23	16.22	4.06	0.55
30.59	22.06	3.22	26.38	30.50	4.07	18.06	3.67	0.49
33.38	44.44	6.70	27.65	32.20	4.48	20.43	4.07	0.55
35.01	50.33	7.59	28.54	27.10	3.62	20.59	4.35	0.60
36.58	57.84	8.71	29.50	26.53	3.48	22.15	9.04	1.19
38.10	55.49	8.36	30.59	24.19	3.24	23.18	12.80	1.66
39.57	59.82	9.00	31.27	25.82	3.39	23.65	14.53	1.89
42.60	57.20	8.00	32.38	27.91	3.72	25.98	18.19	2.44
43.67	51.20	6.96	33.38	34.80	4.55	26.38	18.12	2.43
47.27	50.49	6.87	35.01	47.42	6.17	27.65	24.49	3.27
			36.58	71.24	9.16	28.54	26.65	3.64
			38.10	92.86	11.92	29.50	31.41	4.23
			39.57	117.65	15.10	30.59	31.63	4.41
			42.60	135.19	17.93	31.27	34.80	4.77
			43.67	153.06	19.67	32.38	37.74	5.35
			47.27	208.95	26.82	33.38	40.27	4.40
						33.56	37.55	5.89
						35.01	38.70	5.83
						36.58	37.61	5.66
						38.10	32.28	4.86
						39.57	30.64	4.62
						42.60	31.92	4.36
						43.67	28.19	3.75
						47.27	25.56	3.39

Table A-3 Measured cross section of the ^{nat}Fe + d reactions (continued)

^{nat}Fe(d,x)^{56}Co			^{nat}Fe(d,x)^{57}Co		
E_d (MeV)	σ (mb)	$\Delta\sigma$ (mb)	E_d (MeV)	σ (mb)	$\Delta\sigma$ (mb)
15.31	274.54	36.35	15.31	129.78	18.07
17.30	292.53	38.96	17.30	102.11	14.89
19.06	312.12	41.68	19.06	82.25	11.43
20.59	274.71	36.49	20.71	74.39	9.90
22.28	263.59	35.38	22.28	68.21	9.64
25.98	199.86	26.81	23.76	56.90	7.57
26.38	192.49	25.72	25.98	54.91	7.44
27.65	166.57	22.20	26.38	53.72	7.15
28.54	145.08	19.96	27.65	50.90	6.71
29.50	135.87	17.64	28.54	46.51	6.19
30.59	111.75	15.30	29.50	48.32	6.23
31.27	109.24	14.25	30.59	41.36	5.51
32.38	102.26	13.61	31.27	39.20	5.08
33.56	90.56	11.96	32.38	39.02	5.19
35.01	86.04	11.95	33.56	36.21	4.70
36.58	79.62	11.42	35.01	37.20	4.80
38.10	71.81	9.60	36.58	36.21	4.66
39.57	67.79	9.07	38.10	31.96	4.15
43.67	58.62	7.59	39.57	30.01	4.31
47.27	51.35	6.60	42.60	29.93	3.99
			43.67	29.19	3.77
			47.27	26.70	3.43

Table A-4 Measured cross section of the ^{nat}Ni + d reactions

^{nat}Ni(d,x)^{55}Co			^{nat}Ni(d,x)^{57}Co			^{nat}Ni(d,x)^{60}Cu		
E_d (MeV)	σ (mb)	$\Delta\sigma$ (mb)	E_d (MeV)	σ (mb)	$\Delta\sigma$ (mb)	E_d (MeV)	σ (mb)	$\Delta\sigma$ (mb)
15.25	7.26	0.93	18.06	44.12	6.12	14.23	16.51	2.15
16.23	9.96	1.43	19.77	86.37	11.63	15.25	28.08	3.75
17.16	12.12	1.67	21.38	147.25	20.30	16.23	38.27	5.08
18.06	14.85	2.02	22.91	232.82	31.77	17.16	46.39	6.22
18.93	16.70	2.23	26.66	313.78	41.86	18.06	49.11	6.52
19.77	19.48	2.70	27.31	339.44	46.15	18.93	49.28	6.60
21.38	25.33	3.34	29.42	410.75	55.69	19.77	52.68	7.03
21.81	21.60	2.84	30.12	428.06	55.19	21.38	46.57	6.25
22.91	27.48	3.60	31.50	450.79	60.00	21.81	42.71	5.69
23.92	24.46	3.75	32.10	486.57	63.26	22.91	44.66	5.95
26.66	26.19	3.45	32.69	498.48	64.84	23.92	34.86	5.40
27.31	22.30	3.22	32.76	480.90	62.55	26.66	35.96	4.80
28.30	20.26	2.77	33.25	475.42	63.78	27.31	33.67	4.69
29.42	17.95	2.46	33.95	500.85	64.55	28.30	28.35	3.82
30.12	17.88	2.39	34.76	470.43	60.39	29.42	27.16	3.76
31.50	14.67	2.06	35.55	489.75	64.10	30.12	23.78	3.16
32.10	14.17	1.93	37.10	467.42	60.45	31.50	21.53	2.99
32.69	13.26	2.07	37.63	465.45	60.65	32.10	20.49	2.75
32.76	14.16	2.23	38.61	459.12	62.20	33.25	18.71	2.60
33.25	12.85	1.83	40.07	411.07	52.90	33.95	16.37	2.27
33.95	11.92	1.85	43.22	409.80	55.23	34.76	14.11	2.22
34.76	9.44	1.55	44.28	424.14	54.93	35.55	13.44	1.92
35.55	10.28	1.41	45.33	393.80	52.62	37.10	12.91	2.12
37.10	8.47	1.38	46.45	399.63	53.88	37.63	12.42	1.97
37.63	8.59	1.40	47.84	383.77	49.83	38.61	11.50	1.64
38.61	8.92	1.26				40.07	11.88	1.86
40.07	7.51	1.45				43.22	11.19	1.56
43.22	8.74	1.23				45.33	9.83	1.35
44.28	8.88	1.21				46.45	9.70	1.33
45.33	8.67	1.26						
46.45	8.52	1.21						
47.84	8.79	1.20						

Table A-4 Measured cross section of the ^{nat}Ni + d reactions (continued)

^{nat}Ni(d,x)^{61}Cu		
E_d (MeV)	σ (mb)	$\Delta\sigma$ (mb)
14.23	34.98	4.61
15.25	29.12	4.04
16.23	25.56	3.44
17.16	20.82	3.01
18.06	22.31	3.08
18.93	15.99	2.42
19.77	19.74	2.89
21.38	17.52	2.68
21.81	15.32	2.37
22.91	18.82	2.94
23.92	14.77	2.61
26.66	15.69	2.42
27.31	15.71	2.63
28.30	15.86	2.60
29.42	15.45	2.51
30.12	16.21	2.37
31.50	15.34	2.27
32.69	14.47	2.37
33.25	14.65	2.46
33.95	16.42	2.65
34.76	13.84	2.35
35.55	13.92	2.21
37.10	12.29	1.99
37.63	11.70	1.95
38.61	12.00	1.79
40.07	10.53	1.76
43.22	10.28	1.54
44.28	9.57	1.60
45.33	10.10	1.48
46.45	9.33	1.48
47.84	9.73	1.72

Table A-5 Measured cross section of the ^{nat}Cu + d reactions

^{nat}Cu(d,x)^{62}Zn			^{nat}Cu(d,x)^{63}Zn			^{nat}Cu(d,x)^{61}Cu		
E_d (MeV)	σ (mb)	$\Delta\sigma$ (mb)	E_d (MeV)	σ (mb)	$\Delta\sigma$ (mb)	E_d (MeV)	σ (mb)	$\Delta\sigma$ (mb)
20.30	3.68	0.49	20.30	263.97	36.44	22.75	0.40	0.40
21.54	6.28	0.83	21.54	227.63	31.28	24.31	0.50	0.40
22.75	9.71	1.33	22.75	207.66	28.84	24.92	0.70	0.20
24.31	13.60	1.90	23.88	158.03	21.80	25.44	0.60	0.30
24.92	15.40	2.10	24.31	175.00	25.00	26.88	1.10	0.40
25.44	16.90	2.30	24.92	165.10	22.30	27.45	1.40	0.30
26.88	23.60	3.20	25.44	147.00	20.80	27.92	1.80	0.40
27.45	25.00	3.40	26.88	127.90	18.60	29.28	2.80	0.50
27.92	25.10	3.30	27.45	120.30	16.80	29.81	3.40	0.60
29.28	31.60	4.20	27.92	107.80	15.30	30.26	4.20	0.70
29.81	32.80	4.40	29.28	96.90	14.10	31.53	7.80	1.13
30.26	32.90	4.40	29.81	87.80	12.90	32.04	9.30	1.40
31.53	31.60	4.20	30.26	84.40	12.60	32.46	11.50	1.60
32.04	37.70	5.10	31.53	96.90	14.10	33.68	18.60	2.50
32.46	36.50	4.80	32.04	77.90	11.50	34.15	22.20	3.10
33.68	37.30	5.00	32.46	76.90	11.60	34.31	22.68	3.18
34.15	37.70	5.10	33.68	69.70	10.60	35.19	31.48	4.34
34.31	38.51	5.22	34.15	71.20	11.40	36.04	38.69	5.29
35.19	38.29	5.19	34.31	70.58	10.29	36.89	48.08	6.52
36.04	37.73	5.11	35.19	67.68	9.93	37.72	54.19	7.36
36.89	36.55	4.95	36.04	68.32	10.39	38.54	63.99	8.69
37.72	33.59	4.55	36.89	71.94	10.89	39.35	70.30	9.55
38.54	33.15	4.49	37.72	66.13	10.84	40.15	76.84	10.41
39.35	31.28	4.25	38.54	64.16	10.02	40.99	71.39	9.49
40.15	29.45	3.99	39.35	63.56	9.89	41.86	77.39	10.24
43.68	25.40	3.48	40.15	70.79	11.07	43.68	96.74	12.92
40.99	27.72	3.56	43.68	64.06	9.10	44.74	102.25	13.41
44.74	22.54	2.90	45.78	66.16	9.27	45.78	109.37	14.66
45.78	21.00	2.90	46.89	66.24	9.38	46.89	112.32	15.08
46.89	20.68	2.84				48.27	114.15	14.72
48.27	19.64	2.69						

Table A-5 Measured cross section of the ^{nat}Cu + d reactions (continued)

^{nat}Cu(d,x)^{64}Cu		
E_d (MeV)	σ (mb)	$\Delta\sigma$ (mb)
20.30	105.36	14.64
21.54	107.16	14.85
24.92	130.10	18.00
27.45	140.00	19.30
29.81	156.90	21.60
32.04	161.40	22.20
34.15	174.40	24.00
34.31	172.90	24.48
35.19	175.06	25.11
36.04	194.53	27.43
36.89	166.59	22.90
37.72	156.34	22.35
38.54	172.53	25.01
39.35	163.48	23.82
40.15	157.21	22.36
40.99	160.66	20.94
41.86	152.32	20.32
44.74	150.50	20.15
48.27	136.28	18.26

Table A-6 Measured cross section of the ^{nat}Ta + d reactions

^{nat}Ta(d,x)^{178}Ta			^{nat}Ta(d,x)^{180}Ta		
E_d (MeV)	σ (mb)	$\Delta\sigma$ (mb)	E_d (MeV)	σ (mb)	$\Delta\sigma$ (mb)
28.63	0.14	0.02	25.38	81.19	12.66
30.74	0.49	0.07	25.38	81.19	12.66
31.80	0.77	0.10	26.97	111.67	15.44
33.05	1.26	0.17	26.97	111.67	17.30
33.28	1.77	0.28	27.64	127.40	17.62
33.83	1.43	0.20	27.64	127.40	19.74
34.24	2.21	0.29	28.63	153.55	19.78
35.04	2.77	0.42	28.63	153.55	23.10
35.83	3.44	0.46	29.10	161.21	21.97
37.37	5.03	0.67	29.10	161.21	24.68
37.90	5.53	0.86	30.05	181.43	24.93
38.87	8.45	1.12	30.05	181.43	27.96
39.61	9.55	1.47	30.74	198.87	25.62
40.49	14.69	1.92	30.74	198.87	29.92
45.28	42.62	5.74	31.80	210.17	27.10
48.78	96.95	13.05	31.80	210.17	31.64
			33.05	232.18	30.97
			33.05	232.18	34.99
			33.83	242.18	36.56
			33.83	242.18	36.56
			35.04	214.06	32.46
			37.90	253.40	38.76
			39.61	275.01	42.62
			41.56	251.22	32.42
			45.28	255.78	33.71
			48.78	268.12	37.18

Table A-7 Measured cross section of the ^{nat}W + d reactions

$^{nat}W(d,x)^{181}Re$			$^{nat}W(d,x)^{182}Re$			$^{nat}W(d,x)^{183}Re$		
E_d (MeV)	σ (mb)	$\Delta\sigma$ (mb)	E_d (MeV)	σ (mb)	$\Delta\sigma$ (mb)	E_d (MeV)	σ (mb)	$\Delta\sigma$ (mb)
19.66	286.97	37.95	19.54	256.00	29.52	18.34	486.97	68.25
20.93	335.59	45.11	20.93	232.48	30.23	19.54	477.67	61.75
22.14	386.73	52.42	22.36	247.36	30.13	19.66	489.31	67.85
22.79	385.90	51.60	22.79	242.20	33.00	20.93	492.75	70.34
23.33	379.00	50.00	23.33	232.50	30.90	22.14	565.81	78.26
24.87	451.70	60.00	24.87	249.20	31.30	22.36	538.18	69.57
25.47	485.90	64.90	25.47	277.40	35.00	22.79	422.40	56.40
25.98	440.10	58.00	25.98	271.80	33.70	23.33	391.00	51.60
27.40	473.20	62.90	27.40	311.60	39.10	24.87	369.60	49.10
27.96	479.80	64.10	27.96	350.30	38.70	25.47	371.20	49.60
28.43	448.90	59.20	28.43	358.30	42.60	25.98	307.80	40.60
29.76	434.80	57.80	29.76	395.60	44.80	27.40	267.50	35.60
30.29	449.40	60.00	30.29	410.90	43.20	27.96	253.70	34.00
30.73	387.80	51.10	30.73	383.40	43.20	28.43	232.20	30.70
32.00	403.70	53.70	32.00	399.50	44.40	29.76	239.20	31.90
32.50	416.50	55.60	32.50	408.00	42.30	30.29	229.60	30.70
32.92	382.60	50.40	32.92	381.00	37.40	30.73	207.20	27.40
34.12	392.90	52.20	34.12	372.30	40.40	32.00	238.60	31.80
34.75	462.45	64.48	34.75	371.42	45.79	32.50	253.90	34.00
35.62	461.75	64.36	35.62	371.59	41.09	32.92	241.30	31.90
36.47	482.83	67.07	36.47	349.92	38.44	34.12	272.10	36.10
37.31	536.81	73.78	37.31	326.93	42.61	34.75	305.76	41.43
38.13	528.72	73.03	38.13	306.94	36.59	35.62	322.53	43.67
38.95	527.83	73.09	38.95	284.69	32.02	36.47	347.90	47.29
39.75	499.88	70.18	39.75	252.44	29.62	37.31	363.37	49.27
42.16	543.88	69.84	42.16	253.10	28.79	38.13	367.54	49.83
45.85	508.17	65.26	45.85	277.44	30.51	38.95	368.95	50.02
49.32	416.00	53.43	49.32	359.30	38.11	39.75	362.83	49.19
						42.16	338.08	46.23
						45.85	259.13	35.49
						49.32	187.07	25.56

Table A-7 Measured cross section of the ^{nat}W + d reactions (continued)

$^{nat}W(d,x)^{184}Re$			$^{nat}W(d,x)^{186}Re$			$^{nat}W(d,x)^{187}W$		
E_d (MeV)	σ (mb)	$\Delta\sigma$ (mb)	E_d (MeV)	σ (mb)	$\Delta\sigma$ (mb)	E_d (MeV)	σ (mb)	$\Delta\sigma$ (mb)
19.67	108.54	13.20	22.79	28.70	4.20	22.36	42.23	6.48
22.79	136.60	16.50	23.33	24.30	4.20	22.79	40.70	6.50
23.33	169.10	19.50	24.87	21.00	3.50	23.33	35.00	5.60
24.87	259.90	28.60	25.47	23.00	3.60	24.87	28.90	4.90
25.47	313.70	34.60	25.98	20.90	3.80	25.47	33.30	5.60
25.98	294.20	31.90	27.40	17.10	3.30	25.98	25.00	4.50
27.40	384.10	41.70	27.96	18.80	3.00	27.40	25.20	4.80
27.96	410.70	44.10	28.43	16.90	3.50	27.96	23.80	4.40
28.43	407.10	43.60	29.76	15.70	3.10	28.43	23.30	4.60
29.76	496.00	54.30	30.29	15.00	2.70	29.76	22.70	4.50
30.29	468.70	49.40	30.73	13.30	3.10	30.29	22.40	4.20
30.73	418.50	44.10	32.00	14.30	3.00	30.73	20.30	3.70
32.00	391.50	42.50	32.50	13.60	2.40	32.00	20.70	4.20
32.50	419.50	44.60	32.92	13.40	3.00	32.50	18.50	3.70
32.92	371.40	38.50	34.12	11.60	2.60	32.92	18.10	2.70
34.12	318.60	33.00				34.12	16.50	3.50
34.75	337.11	36.25				34.75	20.35	3.53
35.62	298.00	32.46				35.62	20.12	3.76
36.47	276.10	30.66				36.47	17.25	3.04
37.31	257.23	27.85				37.31	17.65	3.32
38.13	229.67	27.05				38.13	16.15	3.05
38.95	199.66	22.33				38.95	16.74	3.03
39.75	188.19	20.82				39.75	15.65	2.90
						42.16	12.57	2.22
						45.85	9.78	1.94
						49.32	7.02	2.25

Table A-8 Measured cross section of the ^{197}Au + d reaction

^{197}Au(d,x) ^{194}Au		
E_d (MeV)	σ (mb)	$\Delta\sigma$ (mb)
33.74	2.91	0.60
35.21	4.61	0.83
35.93	5.16	0.93
36.64	6.64	1.08
37.33	7.00	1.12
38.03	7.99	1.23
38.71	10.74	1.59
39.38	11.70	1.75

国際単位系（SI）

表１．SI 基本単位

基本量	SI 基本単位	
	名称	記号
長さ	メートル	m
質量	キログラム	kg
時間	秒	s
電流	アンペア	A
熱力学温度	ケルビン	K
物質量	モル	mol
光度	カンデラ	cd

表２．基本単位を用いて表されるSI組立単位の例

組立量	SI 基本単位	
	名称	記号
面積	平方メートル	m^2
体積	立法メートル	m^3
速さ，速度	メートル毎秒	m/s
加速度	メートル毎秒毎秒	m/s^2
波数	毎メートル	m^{-1}
密度（質量密度）	キログラム毎立法メートル	kg/m^3
質量体積（比体積）	立法メートル毎キログラム	m^3/kg
電流密度	アンペア毎平方メートル	A/m^2
磁界の強さ	アンペア毎メートル	A/m
（物質量の）濃度	モル毎立方メートル	mol/m^3
輝度	カンデラ毎平方メートル	cd/m^2
屈折率	（数の） 1	1

表５．SI 接頭語

乗数	接頭語	記号	乗数	接頭語	記号
10^{24}	ヨタ	Y	10^{-1}	デシ	d
10^{21}	ゼタ	Z	10^{-2}	センチ	c
10^{18}	エクサ	E	10^{-3}	ミリ	m
10^{15}	ペタ	P	10^{-6}	マイクロ	μ
10^{12}	テラ	T	10^{-9}	ナノ	n
10^{9}	ギガ	G	10^{-12}	ピコ	p
10^{6}	メガ	M	10^{-15}	フェムト	f
10^{3}	キロ	k	10^{-18}	アト	a
10^{2}	ヘクト	h	10^{-21}	ゼプト	z
10^{1}	デカ	da	10^{-24}	ヨクト	y

表３．固有の名称とその独自の記号で表されるSI組立単位

組立量	SI 組立単位			
	名称	記号	他のSI単位による表し方	SI基本単位による表し方
平面角	ラジアン(a)	rad		$m \cdot m^{-1}=1$(b)
立体角	ステラジアン(a)	sr(c)		$m^2 \cdot m^{-2}=1$(b)
周波数	ヘルツ	Hz		s^{-1}
力	ニュートン	N		$m \cdot kg \cdot s^{-2}$
圧力，応力	パスカル	Pa	N/m^2	$m^{-1} \cdot kg \cdot s^{-2}$
エネルギー，仕事，熱量	ジュール	J	N・m	$m^2 \cdot kg \cdot s^{-2}$
工率，放射束	ワット	W	J/s	$m^2 \cdot kg \cdot s^{-3}$
電荷，電気量	クーロン	C		s・A
電位差（電圧），起電力	ボルト	V	W/A	$m^2 \cdot kg \cdot s^{-3} \cdot A^{-1}$
静電容量	ファラド	F	C/V	$m^{-2} \cdot kg^{-1} \cdot s^4 \cdot A^2$
電気抵抗	オーム	Ω	V/A	$m^2 \cdot kg \cdot s^{-3} \cdot A^{-2}$
コンダクタンス	ジーメンス	S	A/V	$m^{-2} \cdot kg^{-1} \cdot s^3 \cdot A^2$
磁束	ウエーバ	Wb	V・s	$m^2 \cdot kg \cdot s^{-2} \cdot A^{-1}$
磁束密度	テスラ	T	Wb/m^2	$kg \cdot s^{-2} \cdot A^{-1}$
インダクタンス	ヘンリー	H	Wb/A	$m^2 \cdot kg \cdot s^{-2} \cdot A^{-2}$
セルシウス温度	セルシウス度(d)	℃		K
光束	ルーメン	lm	$cd \cdot sr$(c)	$m^2 \cdot m^{-2} \cdot cd=cd$
照度	ルクス	lx	lm/m^2	$m^2 \cdot m^{-4} \cdot cd=m^{-2} \cdot cd$
（放射性核種の）放射能	ベクレル	Bq		s^{-1}
吸収線量，質量エネルギー分与，カーマ	グレイ	Gy	J/kg	$m^2 \cdot s^{-2}$
線量当量，周辺線量当量，方向性線量当量，個人線量当量，組織線量当	シーベルト	Sv	J/kg	$m^2 \cdot s^{-2}$

(a)ラジアン及びステラジアンの使用は、同じ次元であっても異なった性質をもった量を区別するときの組立単位の表し方として利点がある。組立単位を形作るときのいくつかの用例は表４に示されている。
(b)実際には、使用する時には記号rad及びsrが用いられるが、習慣として組立単位としての記号“１”は明示されない。
(c)測光学では、ステラジアンの名称と記号srを単位の表し方の中にそのまま維持している。
(d)この単位は、例としてミリセルシウス度m℃のようにSI接頭語を伴って用いても良い。

表４．単位の中に固有の名称とその独自の記号を含むSI組立単位の例

組立量	SI 組立単位		
	名称	記号	SI 基本単位による表し方
粘度	パスカル秒	Pa・s	$m^{-1} \cdot kg \cdot s^{-1}$
力のモーメント	ニュートンメートル	N・m	$m^2 \cdot kg \cdot s^{-2}$
表面張力	ニュートン毎メートル	N/m	$kg \cdot s^{-2}$
角速度	ラジアン毎秒	rad/s	$m \cdot m^{-1} \cdot s^{-1}=s^{-1}$
角加速度	ラジアン毎平方秒	rad/s^2	$m \cdot m^{-1} \cdot s^{-2}=s^{-2}$
熱流密度，放射照度	ワット毎平方メートル	W/m^2	$kg \cdot s^{-3}$
熱容量，エントロピー	ジュール毎ケルビン	J/K	$m^2 \cdot kg \cdot s^{-2} \cdot K^{-1}$
質量熱容量（比熱容量），質量エントロピー	ジュール毎キログラム毎ケルビン	J/(kg・K)	$m^2 \cdot s^{-2} \cdot K^{-1}$
質量エネルギー（比エネルギー）	ジュール毎キログラム	J/kg	$m^2 \cdot s^{-2} \cdot K^{-1}$
熱伝導率	ワット毎メートル毎ケルビン	W/(m・K)	$m \cdot kg \cdot s^{-3} \cdot K^{-1}$
体積エネルギー	ジュール毎立方メートル	J/m^3	$m^{-1} \cdot kg \cdot s^{-2}$
電界の強さ	ボルト毎メートル	V/m	$m \cdot kg \cdot s^{-3} \cdot A^{-1}$
体積電荷	クーロン毎立方メートル	C/m^3	$m^{-3} \cdot s \cdot A$
電気変位	クーロン毎平方メートル	C/m^2	$m^{-2} \cdot s \cdot A$
誘電率	ファラド毎メートル	F/m	$m^{-3} \cdot kg^{-1} \cdot s^4 \cdot A^2$
透磁率	ヘンリー毎メートル	H/m	$m \cdot kg \cdot s^{-2} \cdot A^{-2}$
モルエネルギー	ジュール毎モル	J/mol	$m^2 \cdot kg \cdot s^{-2} \cdot mol^{-1}$
モルエントロピー，モル熱容量	ジュール毎モル毎ケルビン	J/(mol・K)	$m^2 \cdot kg \cdot s^{-2} \cdot K^{-1} \cdot mol^{-1}$
照射線量（X線及びγ線）	クーロン毎キログラム	C/kg	$kg^{-1} \cdot s \cdot A$
吸収線量率	グレイ毎秒	Gy/s	$m^2 \cdot s^{-3}$
放射強度	ワット毎ステラジアン	W/sr	$m^4 \cdot m^{-2} \cdot kg \cdot s^{-3}=m^2 \cdot kg \cdot s^{-3}$
放射輝度	ワット毎平方メートル毎ステラジアン	$W/(m^2 \cdot sr)$	$m^2 \cdot m^{-2} \cdot kg \cdot s^{-3}=kg \cdot s^{-3}$

表６．国際単位系と併用されるが国際単位系に属さない単位

名称	記号	SI 単位による値
分	min	1 min=60s
時	h	1h =60 min=3600 s
日	d	1 d=24 h=86400 s
度	°	1°=(π/180) rad
分	’	1’=(1/60)°=(π/10800) rad
秒	”	1”=(1/60)’=(π/648000) rad
リットル	l、L	1l=1 $dm^3=10^{-3}m^3$
トン	t	$1t=10^3$ kg
ネーパ	Np	1Np=1
ベル	B	1B=(1/2)ln10(Np)

表７．国際単位系と併用されこれに属さない単位でSI単位で表される数値が実験的に得られるもの

名称	記号	SI 単位であらわされる数値
電子ボルト	eV	$1eV=1.60217733(49) \times 10^{-19}J$
統一原子質量単位	u	$1u=1.6605402(10) \times 10^{-27}kg$
天文単位	ua	$1ua=1.49597870691(30) \times 10^{11}m$

表８．国際単位系に属さないが国際単位系と併用されるその他の単位

名称	記号	SI 単位であらわされる数値
海里		1海里=1852m
ノット		1ノット=1海里毎時=(1852/3600)m/s
アール	a	$1a=1\ dam^2=10^2m^2$
ヘクタール	ha	$1ha=1\ hm^2=10^4m^2$
バール	bar	$1\ bar=0.1MPa=100kPa=1000hPa=10^5Pa$
オングストローム	Å	$1\ Å=0.1nm=10^{-10}m$
バーン	b	$1\ b=100fm^2=10^{-28}m^2$

表９．固有の名称を含むCGS組立単位

名称	記号	SI 単位であらわされる数値
エルグ	erg	$1\ erg=10^{-7}$ J
ダイン	dyn	$1\ dyn=10^{-5}N$
ポアズ	P	$1\ P=1\ dyn \cdot s/cm^2=0.1Pa \cdot s$
ストークス	St	$1\ St=1cm^2/s=10^{-4}m^2/s$
ガウス	G	1 G ^10^{-4}T
エルステッド	Oe	1 Oe ^(1000/4π)A/m
マクスウェル	Mx	1 Mx ^10^{-8}Wb
スチルブ	sb	$1\ sb=1cd/cm^2=10^4cd/m^2$
ホト	ph	$1\ ph=10^4lx$
ガル	Gal	$1\ Gal=1cm/s^2=10^{-2}m/s^2$

表10．国際単位に属さないその他の単位の例

名称	記号	SI 単位であらわされる数値
キュリー	Ci	$1\ Ci=3.7 \times 10^{10}Bq$
レントゲン	R	$1\ R=2.58 \times 10^{-4}C/kg$
ラド	rad	$1\ rad=1cGy=10^{-2}Gy$
レム	rem	$1\ rem=1\ cSv=10^{-2}Sv$
X線単位		$1X\ unit=1.002 \times 10^{-4}nm$
ガンマ	γ	$1\gamma=1\ nT=10^{-9}T$
ジャンスキー	Jy	$1\ Jy=10^{-26}W \cdot m^{-2} \cdot Hz^{-1}$
フェルミ		$1\ fermi=1\ fm=10^{-15}m$
メートル系カラット		1 metric carat = 200 mg = 2×10^{-4}kg
トル	Torr	1 Torr = (101 325/760) Pa
標準大気圧	atm	1 atm = 101 325 Pa
カロリー	cal	
ミクロン	μ	1 μ =1μm=10^{-6}m

（第７版，1998年改訂）